THE PRODUCTION OF ANHYDROUS PROTON CONDUCTING BIOMEMBRANES FOR POLYMER ELECTROLYTE MEMBRANE FUEL CELL APPLICATIONS

by

Ayşe ASLAN

July 2009

THE PRODUCTION OF ANHYDROUS PROTON CONDUCTING BIOMEMBRANES FOR POLYMER ELECTROLYTE MEMBRANE FUEL CELL APPLICATIONS

by

Ayşe ASLAN

A thesis submitted to

the Graduate Institute of Science and Engineering

of

Fatih University

is partial fulfillment of the requirements for the degree of

Master of Science

in

Chemistry

July 2009
Istanbul, Turkey

APPROVAL PAGE

I certify that this thesis satisfies all the requirements as a thesis for the degree of Master of Science.

_____

Assoc. Prof. Dr. Metin TÜLÜ
Head of Department

This is to certify that I have read this thesis and that in my opinion it is fully adequate, in scope and quality, as a thesis for the degree of Master of Science.

_____

Assoc. Prof. Dr. Ayhan BOZKURT
Supervisor

Examining Committee Members

Assoc. Prof. Dr. Ayhan BOZKURT _____

Prof. Dr. Turgay SEÇKİN _____

Asist. Prof. Dr. Ali Ekrem Müftüoğlu _____

It is approved that this thesis has been written in compliance with the formatting rules laid down by the Graduate Institute of Sciences and Engineering.

_____

Assoc. Prof. Dr. Nurullah ARSLAN

Director

July 2009

THE PRODUCTION OF ANHYDROUS PROTON CONDUCTING BIOMEMBRANES FOR POLYMER ELECTROLYTE MEMBRANE FUEL CELL APPLICATIONS

Ayşe ASLAN

M.Sc. Thesis – Chemistry
July 2009

Supervisor: Assoc. Prof. Dr. Ayhan BOZKURT

ABSTRACT

The thin polymeric membrane is the main component of the membrane electrode assembly (MEA) which is sandwiched between catalytic composite electrodes to construct polymer electrolyte membrane fuel cells (PEMFC). In this study, adenine and guanine functional poly(glycidyl methacrylate) have been synthesized. Anhydrous proton conducting properties and thermal properties of phosphoric acid doped and PVPA blends PGMAAdenine and PGMAGuanine were investigated. Poly(glycidyl methacrylate) (PGMA) was prepared by free radicalic polymerization and then modified with adenine and guanine molecules via ring opening of the epoxide ring. The complexed structure of the polymers was confirmed by FT-IR spectroscopy and ^{13}C CP-MAS NMR and elemental analysis studies. Phosphoric acid doped polymers showed lower Tg values and higher proton conductivities than PVPA blends of functional PGMA. (PGMAAdenine)-$(H_3PO_4)_2$ and (PGMAGuanine)-$(H_3PO_4)_{1,5}$ showed a maximum water-free proton conductivity of approximately 0.004 S/cm at 150 ^{0}C and 7 x 10^{-5} S/cm at 150 ^{0}C, respectively.

Further study on the this thesis, thermal and proton conducting properties of complex polymer electrolytes based on Poly(vinylphosphonic acid), VPA and Poly(styrene sulfonic acid) (PSSA), (1-Vinyl-1,2,4-triazole), PVTri were investigated throughout this work. The membrane materials were produced by complexation of PVPA and PSSA with PVTri at various concentrations to get PVTriP$(VPA)_x$ and PVTriP$(SSA)_x$ where x designates the molar ratio of the polymer repeating units and varied from 0.25 to 4. The complexed structure of the polymers was confirmed by FT-IR spectroscopy. The TGA results verified that the presence of PVTri in the complex polymer electrolytes suppressed the formation of phosphonic acid and sulfonic acid anhydrides up to 150 ^{o}C.

The DSC and SEM results demonstrated the homogeneity of the materials. Proton conductivity and water/methanol uptake of these membranes were also measured. PVTriP$(VPA)_2$ showed a proton conductivity of 2.5x 10^{-5} S/cm at 180 ^{o}C in the anhydrous state. After humidification (RH=50 %), PVTri-P$(VPA)_4$ and PVTri-P$(VPA)_2$ showed respective proton conductivities of 0.008 S/cm and 0.022 S/cm at 100 ^{o}C, respectively. Under anhydrous state, maximum proton conductivity of PVTriP$(SSA)_4$ and PVTriP$(SSA)_2$ membranes was measured as 0.015 at 150 ^{o}C and 0.033 S/cm at 120 ^{o}C, respectively.

Keywords: Poly (glycidyl methacrylate), Adenine, Guanine, PVTri, PVPA, PSSA, polymer electrolyte, anhydrous proton conductivity.

POLİMER ELEKTROLİT MEMBRAN YAKIT HÜCRELERİNİN UYGULAMALARI İÇİN NEMSİZ PROTON İLETKEN BİYOMEMBRANLARIN ÜRETİLMESİ

Ayşe ASLAN

Yüksek Lisans Tezi – Kimya
Temmuz 2009

Tez Yöneticisi: Doç. Dr. Ayhan BOZKURT

ÖZ

Polimer elektrolit membranlar katalitik kompozit elektrotlar arasına sandviç edilmesiyle polimer elektrolit membranlı yakıt pilleri (PEMFC) oluşturulmaktadır. Bu tezde yapılan çalışmalarda, adenin ve guanin biyomolekülleriyle fonksiyonel hale getirilmiş olan poli(glisidil metakrilat) polimerleri sentezlenmiştir ve poli(vinilfosfonik asit) kullanılarak blend hale getirilmiş ve fosforik asit ile dop edildikten sonra nemsiz proton iletkenlik özellikleri incelenmiştir. Poli(glisidil metakrilat) (PGMA) serbest radikal polimerizasyonu ile üretilmiş ve sonra epoksi halkası açılarak adenine ve guanin molekülleri ile modifiye edilmiştir. FT-IR, katı hal ^{13}C CP-MAS NMR ve elemental analiz çalışmaları adenine ve guanin moleküllerinin polimer zincirine yüksek oranda immobilize edildiğini doğrulamaktadır. Fosforik asit ile dop edilen polimerler daha düşük Tg ve daha yüksek proton iletkenliğe sahiptir. (PGMAAdenine)-$(H_3PO_4)_2$ ve (PGMAGuanine)-$(H_3PO_4)_{1,5}$ numunelerinin maksimum nemsiz proton iletkenlikleri yaklaşık 150 ^{0}C'de 0.004 S/cm ve 7 x 10^{-5} S/cm'dir.

Diğer bir çalışma olarak, (1-Vinil-1,2,4-triazol), PVTri ile Poli(vinilfosfonik asit), VPA ve Poli(stiren sülfonik asit) (PSSA) etkileştirilerek polimer iyonic çapraz bağlı polimer elektrolit membranların termal ve proton iletkenlik özellikleri incelenmiştir. PVPA ve PSSA polimerlerinin PVTri ile farklı konsantrasyonlarda (0.25-4) kompleksleştrilmesiyle PVTriP$(VPA)_x$ ve PVTriP$(SSA)_x$ polimer elektrolit membranlar sentezlenmiştir. Polimer elektrolitler hazırlanırken PSSA ve PVPA daki sülfonik asit ve fosfonik asit birim sayısı dikkate alınmıştır. Kompleks polimer elektrolitlerin yapısı FT-IR spektroskopisi ile aydınlatılmıştır. TGA sonuçlarına göre PVTriP$(VPA)_x$ 250 ^{o}C'ye kadar, PVTriP$(SSA)_x$ 200 ^{o}C'ye kadar termal olarak kararlıdır. DSC ve SEM analizleri malzemelerin homojen olduğunu göstermiştir. Proton iletkenlikleri ve su/metanol geçirkenlikleri de ölçülmüştür. PVTriP$(VPA)_2$ 180 ^{o}C'de

nemsiz proton iletkenliği yaklaşık olarak 2.5x 10^{-5} S/cm'dir. Nemlendirme işleminden sonra (bağıl nem=%50), PVTri-P$(VPA)_4$ ve PVTri-P$(VPA)_2$ membranlarının iletkenlik değerleri 100 ^{o}C'de, 0.008 S/cm ve 0.022 S/cm olarak ölçülmüştür. PVTriP$(SSA)_4$ ve PVTriP$(SSA)_2$ membranlarının nemsiz proton iletkenlikleri 0.015 (150 ^{o}C) ve 0.033 S/cm (120 ^{o}C) olarak ölçülmüştür.

Anahtar Kelimeler: Poli (glisidil metakrilat), Adenin, Guanin, PVTri, PVPA, PSSA polimer elektrolit, nemsiz proton iletkenlik.

Dedicated to my parents

ACKNOWLEDGEMENTS

First of all, I would like to express my sincere appreciation to my supervisor Assoc. Prof. Dr. Ayhan Bozkurt, for providing me all the opportunities, for his guidance and encouragement throughout the research.

Endless thanks to Prof. Dr. Turgay Seçkin for good communication and encouragement.

Thanks to TUBİTAK (BİDEB-2227) for scholarship throughout this research and support from TUBİTAK- under contract number TABG-108T103.

For technical support in the laboratory, I am grateful to Sevim Ü. Çelik.

Thanks go to Ümit Akbey and Christoph Sieber from Max-Planck Institute for solid state ^{13}C CP-MAS NMR and studies respectively.

Special thanks to my friends Hilal Yanardağ and Aslıhan Sezgin for moral support and encouragements .

I express my thanks and appreciation to my family for their understanding, motivation and patience throughout my education.

TABLE OF CONTENTS

LIST OF TABLES

TABLE

LIST OF FIGURES

FIGURE

CHAPTER 1

INTRODUCTION

Polymer electrolyte membrane fuel cell (PEMFC) is one of the promising power systems that can be utilized in many applications such as electric vehicles, mobile phones, and on-site power generators as the power needs gets more and more demanding from these systems (Kerres, 2001, Rikukawa and Sanui, 2000, Kreuer, 2001). Polymer electrolyte membrane is the separator material in those devices that inhibit the fuel (gas) diffusion and permit protons diffuse from anodic to cathodic side (Schuster et al., 2004, Wainright et al., 1995, Schuster et al., 2003, Smitha et al., 2005)

Although commercial perfluorosulfonic acid (Nafion®) has been promising membrane in terms of proton conductivity, it has some disadvantages, i.e., external humidification, high material cost and high methanol crossover. There has been an increasing research on the development of hydrocarbon based proton conducting polymer electrolytes in order to sustain adequate proton conductivity under low humidity, exceeding 100 ^{o}C (Chang et al., 2003, Shen et al., 2007, Bozkurt and Meyer, 2001).

The operation of fuel cells at higher temperatures provides some advantages such as, improvement of CO tolerance of platinum catalyst, improve mass transportation, increase reaction kinetics and simplify the water management and gas humidification (Kreuer, 2001, Schuster et al., 2003)

Thereafter, polymer/acid complexes have been considered as alternative materials for proton conductors in the anhydrous state (Shen et al., 2007, Schechter et al., 2002, Yang et al., 2001, Kreuer et al., 1998). In these complexes, strong acid/polymer interaction by way of hydrogen bonding leads to homogeneous systems and proton conduction occur over the bronsted acid-base pairs (Chang et al., 2003). Desirable high proton

conductivity can only be reached at higher acid compositions in these systems that would result in leaching out of small molecular weight proton solvents during prolonged usage in fuel cells.

Another recent approach was doping of acidic polymers with amphoteric heterocyclic structures such as imidazole (Im) (Sevil et al., 2004, Yamada and Honma, 2003, Sen et al., 2008), pyrazole (Py) (Yamada and Honma, 2003), benzimidazole (BmIm) (Bozkurt et al., 2003) and triazole (Tri) (Wycisk et al., 2006). In these systems, the host polymer improves the mechanical properties and thin freestanding films can be produced. Polymers also function as a proton source by means of supplying protons to heterocyclic protogenic solvents that enhance the defect-type proton conductivity. Although the use of these heterocyclic systems as composite components in an acidic polyelectrolyte was useful for the development of high temperature resistant films, the solvent leaching out could be problem for prolonged fuel cell application. Thus, immobilization of the proton solvents can be carried out via copolymerization of acidic monomer with heterocyclic comonomer. It was previously reported that copolymers of 4(5)-vinylimidazole yielded low conductivities due to ionic complexation which blocked the free nitrogens and long range proton diffusion was inhibited (Hasiotis et al., 2001). To solve complexation and blocking of free nitrogens in the heterocyclic ring, the use of triazole based polymer would be interesting and may solve the blocking as well as dopant leaching out problems.

An interesting approach can be the proton solvent comprising functional polymers that are thermally stable and having proton transport channel. From this point of view, polymer membranes including adenine and guanine units would be interesting where these biopolymers can be used as the proton charge carriers in the membrane under anhydrous condition. The utilization of biopolymers as a membrane material was reported in an earlier study (Nakayama et al., 2001). In this context, Park at al reported the DNA/PEI and DNA/PEO proton conducting systems (Park, 2008).

Blending of high molecular weight acidic and basic polymers would be alternative to tackle the leaching out problem. Proton conducting blend membranes has been produced by blending of Nafion and polybenzimidazole (PBI) by solution casting (Pasupathi et al., 2008). In fact, the basic character of the imidazole nitrogen caused partially or completely transfers of the protons from the sulfonic group through

hydrogen bonding network. On the other hand, a decrease in proton conductivity has been reported as a consequence of the involvement of some fraction of the sulfonic acid groups in PBI cross-linking. The proton conductivity as well as methanol permeability of the blends decreased through increasing PBI content (Pasupathi et al., 2008).

In another approach, Hasiotis et al. produced proton conducting polymer electrolytes based on the sulfonated polysulfones (SPSF) and polybenzimidazole (PBI) by doping with phosphoric acid. The water uptake of the blends increased with increasing PBI content. Furthermore, the doping level increased with increasing acid concentration, temperature and PBI content. Due to increasing temperature and doping level, ionic conductivity of the membranes increased. However, almost no effect of relative humidity on the proton conductivity was observed (Zhang et al., 2008).

Pasupathi et al. studied acid-base polymer blend based on sulfonated poly(etheretherketone) (SPEEK) and poly(benzimidazole) (PBI) (Celik et al., 2008). They compared thermal stability, water uptake, conductivity of the blend membrane to that of Nafion. The conductivity of Nafion was found to be better than SPEEK/PBI membrane; nevertheless, the thickness of SPEEK/PBI membranes can be reduced considerably. The SPEEK/PBI membrane with a thickness of 55 μm showed a noteworthy upgrading in the DMFC performance as compared to Nafion 117. The water uptake of the membrane increases with temperature.

Zhang et. al. also studied highly sulfonated poly(aryl ether ether ketone) (SPEEK) and polybenzimidazole (PBI) acid–base composite membranes. It has been seen that the proton conductivity of the composite membranes depends on the PBI content. The thermal stability and mechanical properties of the SPEEK membranes increased with increasing PBI content. The water uptake of the membrane and proton conductivity decreases with increasing PBI content whereas increased with increasing temperature (Vink, 1981).

The use of poly(1-vinyl-1,2,4-triazole, PVTri, as a blend component with Poly(styrene sulfonic acid) would be interesting since PVTri bears triazole as repeating and showed high proton conductivity when it is doped with phosphoric acid. In addition, PVTri is thermally as well as electrochemically stable polymer and it can be used for high temperature applications (Bozkurt, 2005). The polymer blends consisting of acidic and

heterocyclic polymers which may allow long range proton transport via structure diffusion.

In this work, anhydrous proton conducting properties and thermal properties of PVPA functional and phosphoric acid doped PGMAAdenine and PGMAGuanine were investigated. Poly(glycidyl methacrylate) (PGMA) was prepared by free radicalic polymerization and then modified with adenine and guanine molecules via ring opening of the epoxide ring. The complexed structure of the polymers was confirmed by FT-IR spectroscopy and ^{13}C CP-MAS NMR and elemental analysis studies. The polymer were characterized via FT-IR, TG, DSC and SEM. Proton conducting properties of the copolymers were investigated by impedance analyzer and the results are discussed and compared with previously reported systems.

The synthesis of novel membranes based on the ionically crosslinked PVTri-PVPA systems and PVTri-PSSA systems were discussed. The materials were fabricated at several molar ratios to analyze the effect of PVPA and PSSA contents on the conductivity of final product. The polymer electrolytes PVTriP$(VPA)_x$ and PVTriP$(SSA)_x$ were characterized via FT-IR, TG, DSC and SEM. Proton conducting properties of the copolymers were investigated by impedance analyzer and the results are discussed and compared with previously reported systems.

CHAPTER 2

2.1 FUEL CELLS

Fuel cells are electrochemical devices that convert the chemical energy of a reaction directly into electrical energy. The basic physical structure or building block of a fuel cell consists of an electrolyte layer in contact with a porous anode and cathode on either side. A schematic representation of a fuel cell with the reactant/product gases and the ion conduction flow directions through the cell is shown in Fig. 2.1.

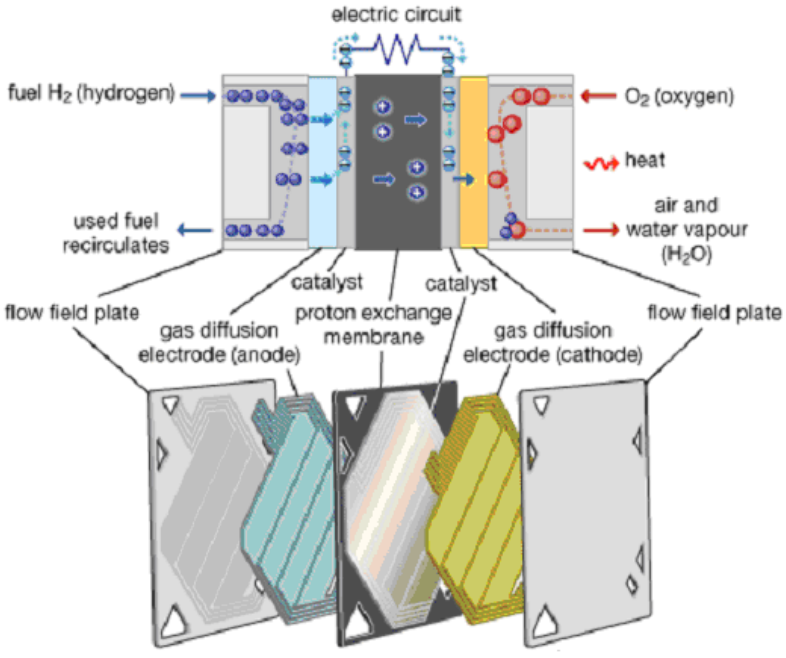

Anode Reactions:	$2H_2 => 4H+ + 4e-$
Cathode Reactions:	$O_2 + 4H+ + 4e- => 2\ H_2O$
Overall Cell Reactions:	$2H_2 + O_2 => 2\ H_2O$

Figure 2.1 Schematic illustration of an individual fuel cell (Encyclopedia Britannica , 2007)

In a typical fuel cell, gaseous fuels are fed continuously to the anode (negative electrode) compartment and an oxidant (i.e., oxygen from air) is fed continuously to the cathode (positive electrode) compartment; the electrochemical reactions take place at the electrodes to produce an electric current. A fuel cell, although having components and characteristics similar to those of a typical battery, differs in several respects. The battery is an energy storage device. The maximum energy available is determined by the amount of chemical reactant stored within the battery itself. The battery will cease to produce electrical energy when the chemical reactants are consumed (i.e., discharged). In a secondary battery, the reactants are regenerated by recharging, which involves putting energy into the battery from an external source. The fuel cell, on the other hand, is an energy conversion device that theoretically has the capability of producing electrical energy for as long as the fuel and oxidant are supplied to the electrodes. Fig. 2.1 is a simplified diagram that demonstrates how the fuel cell works. In reality, degradation, primarily corrosion, or malfunction of components limits the practical operating life of fuel cells. Note that the ion specie and its transport direction can differ, influencing the site of water production and removal, a system impact. The ion can be either a positive or a negative ion, meaning that the ion carries either a positive or negative charge (surplus or deficit of electrons). The fuel or oxidant gases flow past the surface of the anode or cathode opposite the electrolyte and generate electrical energy by the electrochemical oxidation of fuel, usually hydrogen, and the electrochemical reduction of the oxidant, usually oxygen (Fuel Cell Handbook, 2000).

A variety of fuel cells are in different stages of development. They can be classified by use of diverse categories, depending on the combination of type of fuel and oxidant, whether the fuel is processed outside (external reforming) or inside (internal reforming) the fuel cell, the type of electrolyte, the temperature of operation, whether the reactants are fed to the cell by internal or external manifolds, etc. The most common classification of fuel cells is by the type of electrolyte used in the cells and includes 1) polymer electrolyte fuel cell (PEFC), 2) alkaline fuel cell (AFC), 3) phosphoric acid fuel cell (PAFC), 4) molten carbonate fuel cell (MCFC), 5) intermediate temperature solid oxide fuel cell (ITSOFC), and 6) tubular solid oxide fuel cell (TSOFC). These fuel cells are listed in the order of approximate operating temperature, ranging from ~80 ^{o}C for PEFC, ~100 ^{o}C for AFC, ~200 ^{o}C for PAFC, ~650 ^{o}C for MCFC, ~800 ^{o}C for ITSOFC, and 1000 ^{o}C for TSOFC. The operating temperature and useful life of a fuel

cell dictate the physicochemical and thermomechanical properties of materials used in the cell components (i.e., electrodes, electrolyte, interconnect, current collector, etc.). Aqueous electrolytes are limited to temperatures of about 200 ^{o}C or lower because of their high water vapor pressure and/or rapid degradation at higher temperatures. The operating temperature also plays an important role in dictating the type of fuel that can be used in a fuel cell. The low-temperature fuel cells with aqueous electrolytes are, in most practical applications, restricted to hydrogen as a fuel. In high-temperature fuel cells, CO and even CH_4 can be used because of the inherently rapid electrode kinetics and the lesser need for high catalytic activity at high temperature. However, descriptions later in this section note that the higher temperature cells can favor the conversion of CO and CH_4 to hydrogen, then use the equivalent hydrogen as the actual fuel (Fuel Cell Handbook, 2000).

2.1.1 Polymer Electrolyte Fuel Cell (PEFC)

The electrolyte in this fuel cell is an ion exchange membrane (fluorinated sulfonic acid polymer or other similar polymer) that is an excellent proton conductor. The only liquid in this fuel cell is water; thus, corrosion problems are minimal. Water management in the membrane is critical for efficient performance; the fuel cell must operate under conditions where the byproduct water does not evaporate faster than it is produced because the membrane must be hydrated. Because of the limitation on the operating1-4 temperature imposed by the polymer, usually less than 120 ^{o}C, and because of problems with water balance, a H_2-rich gas with minimal or no CO (a poison at low temperature) is used. Higher catalyst loading (Pt in most cases) than that used in PAFCs is required for both the anode and cathode (Fuel Cell Handbook, 2000).

2.1.2 Phosphoric Acid Fuel Cell (PAFC)

Phosphoric acid concentrated to 100 % is used for the electrolyte in this fuel cell, which operates at 150 to 220 ^{o}C. At lower temperatures, phosphoric acid is a poor ionic conductor, and CO poisoning of the Pt electrocatalyst in the anode becomes severe. The relative stability of concentrated phosphoric acid is high compared to other common acids; consequently the PAFC is capable of operating at the high end of the acid temperature range (100 to 220 ^{o}C). In addition, the use of concentrated acid (100 %)

minimizes the water vapor pressure so water management in the cell is not difficult. The matrix universally used to retain the acid is silicon carbide, and the electrocatalyst in both the anode and cathode is Pt (Fuel Cell Handbook, 2000).

2.2 PROTON CONDUCTION MECHANISMS

A proton conductor is an electrolyte, typically a solid electrolyte, in which movable hydrogen ions (protons) are the primary charge carriers. Proton conductors are usually composed of polymer or ceramic because the pore size is small enough that larger negative ions are locked into the solid matrix, and only very small ions (positive hydrogen ions — bare protons) can participate in a direct current. Proton conductors are usually solid materials. When in the form of thin membranes, proton conductors are an essential part of small, inexpensive fuel cells.

Proton conduction was first suggested by Alfred Rene Jean Paul Ubbelohde (14 December 1907 - 7 January 1988) and S.E. Rogers. Water is the best solvent for protons and exhibits unusually high equivalent conductivity of protons, which exceeds the hydrodynamic limit by a factor of 4.5 under ambient conditions. The process for proton transport in water is explained by “Grotthuss mechanism" (Grotthuss, 1806, Kreuer, 1997) also called “hopping mechanism” or “chain mechanism” or “structure diffusion”. The proton transport comprises rapid intermolecular proton transfers (Hopping) down a chain of hydrogen bonds where the transfer events are assumed to be highly correlated, and reorientation of water dipoles in order to produce a configuration which allows for the next hopping event (Grotthuss, 1806, Kreuer, 1997).

The first process leads to a polarization of the hydrogen bond chain, i.e. to a local relative charge displacement, but not to DC conductivity. The second process causes the depolarization of the chain by reorientation of the water dipoles. The mechanism of proton migration in water has been studied extensively (Eigen, 1964, Agmon, 1995, Agmon, 1996). Basically, for a fast Grotthuss type mechanism, it must enable the formation of protonic defects and provide strongly fluctuating proton donor and acceptor functions in an otherwise non-polar environment. The latter avoids strong solvent effects that tend to suppress proton transfer reactions (Kreuer, 1997, Kreuer , 1996). However, this mechanism cannot explain all abnormal proton conductive

systems. Based on NMR spectra and self-diffusion coefficients, Kreuer et al. (Kreuer et al., 1982) proposed "Vehicle mechanism", also called molecular diffusion, for the interpretation of the conductivity of fast proton conductors such as zeolites, Nafion etc. According to this model the proton does not migrate as H^+ but as H_3O^+, NH_4^+, etc., bonded to a " vehicle" such as H_2O, NH_3, etc. (Fig. 2.2) The "unloaded" vehicles move in the opposite direction. Hydrogen bond is not necessary for proton transport with this model.

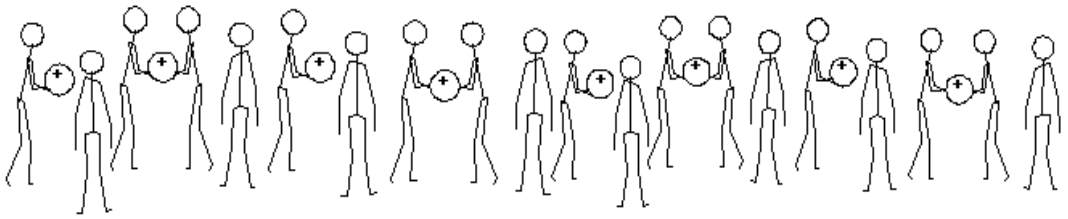

Grotthuss Mechanism

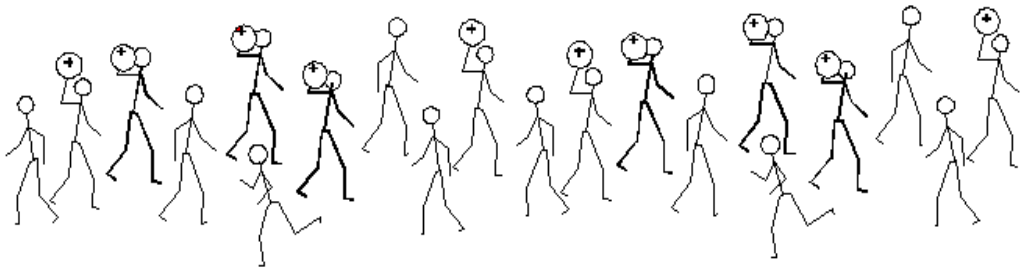

Vehicle Mechanism

Figure 2.2 Schematic representation of phenomena involved in proton conduction mechanisms (Kreuer et al., 1982).

In some systems, the conduction mechanism is contributed by these two models together. Also, the conduction mechanism can change from one model to another model based on the temperature and concentration of the system. For example, in concentrated aqueous solutions of acids such as aqueous HCl, the proton conduction can be well explained by vehicle mechanism. However, if the acid solutions are diluted, i.e. increasing solvent (H_2O) concentration, there is an increasing contribution of structure

diffusion to the overall conductivity, i.e. both of the mechanisms (the mixed mechanism) exist for proton conduction. (Kreuer et al., 1992). Kreuer distinguished the molecular diffusion (vehicle mechanism) and structure diffusion (Grotthuss mechanism) of proton by measuring the self-diffusion coefficients by means of the PFG-NMR technique. (Kreuer, 1996, Kreuer et al., 1992, Dippel and Kreuer, 1991, Bozkurt et al., 1999). Basically, in anhydrous oxo-acids such as H_3PO_4 (Dippel et al., 1993) solid acidic salts of oxo-acids such as $CsHSO_4$ (Cuddeback et al., 1953) and $Zr(HPO_4)_2$ (Alberti et al., 1984) or oxo-acid/polymer blends such as BPEI/$0.5H_2SO_4$ (Lassegues et al., 1989), the proton conductivity can be entirely explained by structure diffusion. In hydrated acidic polymers such as Nafion (Slade et al., 1983), proton conductivity is controlled by molecular diffusion. However, the boiling point of water limits the usage of water as a proton solvent at high temperature. H_3PO_4, due to the formation of 3D polyphosphoric acid network for proton transport at high temperatures and anhydrous environment, is the best solvent for proton at high temperatures and anhydrous conditions. It has been demonstrated that in highly viscous anhydrous phosphoric acid, 98% of the total conductivity arises from structure diffusion of proton (Dippel et al., 1993). Recently, Kreuer (Kreuer et al., 1998) proposed that imidazole, benzimidazole and pyrazole could conduct proton as water does when ionized. After Kreuer's work, a series of work has been done with imidazole of benzimidazole as proton conductor (Ma, 2004).

Phosphoric acid, which can form 3-D hydrogen bonding network due to its special structure, is a very good proton conductive medium. The super-cooled melted pure acid has a conductivity of 0.053 S/cm at 30^{o}C, and this high value is known to come from the extensive self-ionization of H_3PO_4 (Greenwood and Thompson, 1959, Munson, 1964). Structure diffusion was proposed as the operating fast conduction and diffusion mechanism in fused phosphoric acid, where the transference number of proton is close to 1 (≈0.975) (Dippel et al., 1993). Addition of water increases the dissociation, decreases the viscosity therefore brings the conductivity to a maximum of 0.27 S/cm for 45 % acid by weight (Chin and Chang, 1989). Further dilution decreases the number of charge carriers more rapidly than the viscosity, and the conductivity drops finally to the value of pure water. Phosphoric acid can be regarded as a mixture of P_2O_5 and H_2O. At high temperatures, phosphoric acid undergoes auto-dehydration process in addition to the self-dissociation process. The dehydration is reversible at low temperatures if water

is provided. Therefore, phosphoric acid can conduct proton at high temperatures and very low relative humidity by forming polyphosphoric acid network.

It is well known that proton conducing polymer electrolyte can be obtained by doping polymers bearing basic groups such as ether, alcohol, imine, amide or imide with strong acids such as H_3PO_4 or H_2SO_4. H_2SO_4 is more acidic and oxidative than H_3PO_4 and tends to form a salt with a basic site in the polymer thus decreases the concentration of the proton charge carrier. Moreover, the thermal stability of a H_2SO_4 doped polymer is not good due to its oxidizing property. H_3PO_4 is a relatively weak acid. It interacts with the polymer through hydrogen bond or proton transfer reaction depending on the basicity of the polymer.

In acid/polymer systems, the polymer has two functions: on one hand, it has to be sufficiently basic to dissolve and complex with the acid, i.e. it acts as a solvent in which the acid undergoes some dissociation. On the other hand, excess acid is usually needed to obtain a high conductivity. Thus the polymer acts as a matrix to retain the excess acid. However, most of these materials suffer from fundamental limitations such as insufficient chemical stability (e.g. hydrolysis of ethers or amides) or low mechanical stability, especially at higher temperatures or with excess acid. Films with good thermal and mechanical stabilities for high temperature application can be obtained from polymers with high glass transition temperatures such as polybenzimidazole. However, the segmental movement of polymer can assist the proton conductivity so that flexible polymers with low glass transition temperatures are preferred (Ma, 2004).

2.3 POLYMER MEMBRANES

2.3.1 HYDRATED PROTON CONDUCTING MEMBRANES

In general, proton-conducting polymers are usually based on polymer electrolytes, which have negatively charged groups attached to the polymer backbone. These polymer electrolytes tend to be rather rigid and are poor proton conductors unless water

is absorbed. The proton conductivity of hydrated polymer electrolytes dramatically increases with water content and reaches values of 10^{-2}-10^{-1} S cm^{-1}.

The first PEFC used in an operational system was the GE-built 1 kW Gemini power plant (Zawodzinski et al., 1993). This system was used as the primary power source for the Gemini spacecraft during the mid-1960s. The performances and lifetimes of the Gemini PEFCs were limited due to the degradation of poly(styrene sulfonic acid) membrane employed at that time. The degradation mechanism determined by GE was generally accepted until the present time. It was postulated that HO_2 radicals attack the polymer electrolyte membrane. The second GE PEFC unit was a 350 W module that powered the Biosatellite spacecraft in 1969. An improved Nafion® membrane manufactured by DuPont was used as the electrolyte. The performance and lifetime of PEFCs have significantly improved since Nafion® was developed in 1968. Lifetimes of over 50,000 h have been achieved with commercial Nafion® 120 (Rikukawa and Sanui, 2000).

As seen in Fig. 2.3, the Yeager Three Phase Model is a phenomenological based model. This model is based on a three-phase clustered system with interconnecting channels within the polymer. The three regions consist of (A) a fluorocarbon backbone, some of which is microcrystalline, (B) an interfacial region of relatively large fractional void volume containing some pendant side chains, some water, and those sulfate or carboxylic groups and counter ions which are not in clusters, and (C) the clustered regions where the majority of the ionic exchange sites, counter ions, and sorbed water exists (Yeager and Eisenberg, 1982; Brookman and Nicholson, 1986).

From experimental means, such as, small-angle x-ray scattering (SAXS) it has been determined that the phase-separated morphology is on the order of 30-50Å Bragg spacing. However, upon hydration, Nafion® with its unique ability to sorb relatively large amounts of water, can increase its dry weight by as much as 50 percent or more depending upon equivalent weight, counter ion, and temperature. Upon hydration, however, cluster diameter and the number of exchange sites are thought to increase, leading to fewer, larger clusters.

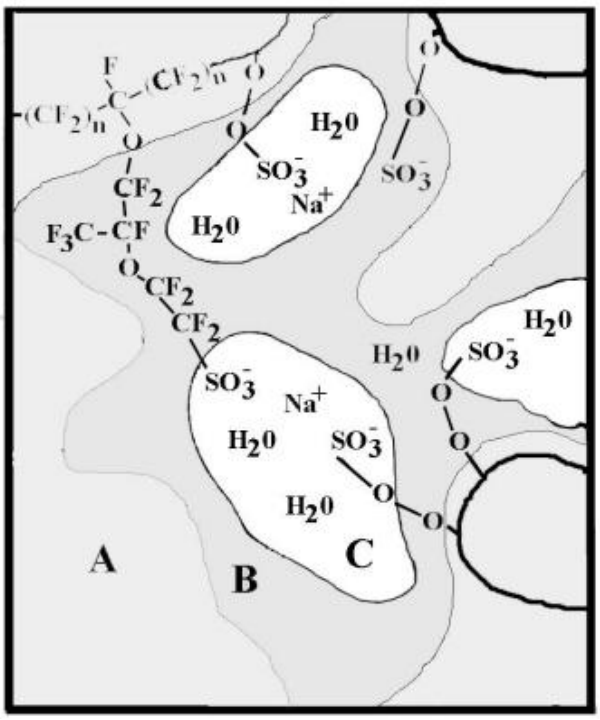

Figure 2.3 The Yeager 3 Phase Model of Nafion® Clusters (Yeager and Eisenberg, 1982).

Nafion® 117 and 115 have equivalent repeat unit molecular weights of 1100 and thicknesses in the dry state of 175 and 125 μm, respectively. Nafion® 120 has an equivalent weight of 1200 and a dry state thickness of 260 μm. Ballard Technologies Corporation showed the possibility of the application of PEFC for electric vehicles by using experimental perfuorinated membranes developed by Dow Chemical. Development of PEFC has been accelerated year by year after the report of Ballard Technologies Corporation. The Dow membrane has an equivalent weight of approximately 800 and a thickness in the wet state of 125 mm. In addition, Flemion® R, S, T, which have equivalent repeat unit molecular weights of 1000 and dry state thicknesses of 50, 80, 120 μm, respectively, were also developed by Asahi Glass Company (Watkins et al., 1993). Asahi Chemical Industry manufactured a series of Aciplex®-S membranes, which have equivalent repeat unit molecular weights of 1000-1200 and dry state thicknesses of 25-100 μm.

These perfuorinated ion exchange membranes including Neosepta-Fw (Tokuyama) and Gore-Selectw (W. L. Gore and Associates, Inc.) have been developed

for chlor-alkali electrolysis. The water uptake and proton transport properties of this type of membrane have signifcant effects on the performance of PEFCs. These membranes have water uptakes of above 15 $H_2O/-SO_3H$, and maximizing membrane water uptake also maximizes the proton conductivity.

In general, conductivities can reach values of 10^{-2}-10^{-1} S cm^{-1}. All of these membranes possess good thermal, chemical, and mechanical properties due to their perfuorinated polymer backbones. A limiting factor in PEFCs is the membrane that serves as a structural framework to support the electrodes and transport protons from the anode to the cathode. The limitations to large-scale commercial use include poor ionic conductivities at low humidities and/or elevated temperatures, a susceptibility to chemical degradation at elevated temperatures and finally, membrane cost. These factors can adversely affect fuel cell performance and tend to limit the conditions under which a fuel cell may be operated. For example, the conductivity of Nafion® reaches up to 10^{-2} S cm^{-1} in its fully hydrated state but dramatically decreases with temperature above the boiling temperature of water because of the loss of absorbed water in the membranes. Consequently, the development of new solid polymer electrolytes, which are cheap materials and possess sufficient electrochemical properties, have become one of the most important areas for research in PEFC and FCEV (Rikukawa and Sanui, 2000).

2.3.2 ANHYDROUS PROTON CONDUCTIVE MEMBRANES

Proton exchange membrane (PEM) fuel cells have gained prominence after they become applicable to various technological areas particularly on portable power generating systems. In general, polymer based proton conducting materials can be categorized according to the temperature range in which they exhibit high proton conductivity.

The first class of materials that can be utilized in the temperature range 25-100°C because their conductivity depends on water content. Within this family of polymers, hydrated perfluorosulfonic acid membranes such as Nafion®, well-established low temperature materials since 1960. These materials are typically phase separated into

hydrophilic/hydrophobic domains and conductivity occurs via transport of dissociated protons by the dynamics of water (Kreuer et al., 1993). These hydrated systems have been used as the polymer electrolytes in hydrogen/oxygen polymer electrolyte fuel cells (PEMFCs) due to excellent chemical and mechanical stability as well as high proton conductivity (Rikukawa and Sanui, 2000, Motupally et al., 2000, Costamagna and Srinivasan, 2001). However, there are several limitations in perfluorosulfonic acid membranes, which retard spread industrial application. The major disadvantages are high cost of the membrane, high operation temperature, high methanol permeability when used in direct methanol fuel cells (DMFCs) and difficult recycling and disposal (Kreuer, 2001, Miyake et al., 2001).

Recently, operation of PEMFCs at intermediate temperature, particularly between 80-180°C has been considered to provide several advantages such as improved carbon monoxide tolerance, higher energy efficiency, and simplified heat managements (Ianniello et al., 1994, Antonucci et al., 1999). In this context, second class of polymer electrolyte membranes are considered as alternative materials that have almost no dependence on humidity and can maintain high proton conductivity (~0.01 S/cm) at medium temperatures. In general, there are three different approaches toward anhydrous PEMs in terms of their chemical structure and conductivity mechanisms:

.

a) Polymer-acid complexes. These are based on polymer networks which contain ether, amide, amine or imino groups are doped with strong acids such as H_3PO_4 or H_2SO_4.
b) Intrinsic proton conductors based on homopolymers, copolymers, and polymer networks produced by tethering the heterocyclic proton solvent.
c) Polymer/heterocycle hybrid electrolytes. In principle, these materials consists of acidic host matrix that forms complexes with amphoteric heterocycles and conduction occurs through protonic defects.

CHAPTER 3

EXPERIMENTAL

3.1 SYNTHESIS OF ADENINE AND GUANINE FUNCTIONAL PGMA (PGMAADENINE AND PGMAGUANINE)

3.1.1 Chemicals

Glycidyl methacrylate (>97%) (Fig. 3.1), Adenine (>99%) (Fig. 3.2) and Guanine (>99%) (Fig. 3.3) were supplied from SigmaAldrich Chemical Company. Ortho-Phosphoric acid (>99%), Toluene (>99%), Diethlyether (>99.5%) and DMSO (>99.5%) were purchased from Merck. Azobisisobutyronitrile (AIBN; Merck) was recrystallized from THF prior to use. Vinylphosphonic acid (> 95%, Fluka), alpha, alpha'-Azodiisobutyramidin Dihydrochlorid (AIBHC, >%98 Fluka) were obtained from Fluka and they are all reagent grade and were used as received.

3.1.2 Synthesis of Poly (glycidyl methacrylate), PGMA

Poly (glycidyl methacrylate) (Fig. 3.1) was produced by free radical polymerization of glycidyl methacrylate (5.0 g) in toluene (100 ml) using AIBN (1% mol) as initiator. The reaction mixture was purged with nitrogen and the polymerization reaction was performed at 75 ^{0}C for 4 h. Transparent solution of the polymer was precipitated in diethyl ether and the product was dried at 50 ^{0}C under vacuum (Celik et al., 2008).

Figure 3.1 Synthesis of PGMA

3.1.3 Synthesis of PGMAAdenine

Adenine (Mw=135 g/mol) and PGMA were dissolved in DMSO to get PGMAAdenine. The molar ratio of adenine to PGMA was varied from 1:1, 1:1.1 and 1:1.2. The temperature was set to 105 ^{0}C and the mixture was stirred for 24 h (Fig. 3.2). The PGMAAdenine were obtained after precipitation with THF and washed with hot water to remove excess adenine. After washing , it was filtered and dried at 50 ^{0}C under vacuum. Yellow and rigid polymers were obtained. Polymers are insoluble in common organic solvents and in aqeous medium.

Figure 3.2 Synthesis of PGMAAdenine

Poly(vinyl phosphonic acid) was produced by free radical polymerization of vinyl phosphonic acid as discussed in an earlier study (Bingöl, 2006). PGMAAdenine and PVPA were dissolved in DMSO. A stoichiometric amounts of PGMAAdenine and PVPA solutions (PGMAAdenine-$(PVPA)_x$); x=0.5, 1, 1.5, 2 (i.e. x is the number of moles of PVPA per moles of adenine unit in the polymer) were mixed. Rigid polymer membranes were obtained.

Doping was performed by dispersing the polymer in DMSO, then adding phosphoric acid with different ratios, x=0.5, 1, 1.5, 2 (i.e. x is the number of moles of acid per moles of adenine unit in the polymer). After evaporating the solvent, polymers were dried completely in a vacuum oven. Rigid polymer membranes were obtained.

3.1.4 Synthesis of PGMAGuanine

Guanine (Mw=151 g/mol) and PGMA were dissolved in DMSO to get PGMAGuanine. The molar ratio of guanine to PGMA was varied from 1:1, 1:1.1 and 1:1.2. The temperature was set to 140 ^{0}C and the mixture was stirred for 24 h (Fig. 3.3). After the reaction was completed, excess guanine precipitated in reaction flask. The resulting mixture was filtered to remove excess guanine and dialized against water to remove excess PGMA. The PGMAGuanine were obtained after dializing. It was dried at 50 ^{0}C under vacuum. Brown and rigid polymers were obtained. Polymers are insoluble in common organic solvents and in aqeous medium.

Figure 3.3 Synthesis of PGMAGuanine

Poly(vinyl phosphonic acid) was produced by free radical polymerization of vinyl phosphonic acid as discussed in an earlier study (Bingöl, 2006). PGMAGuanine and PVPA were dissolved in DMSO. A stoichiometric amounts of PGMAGuanine and PVPA solutions PGMAGuanine-$(PVPA)_x$); x=0.5, 1, 1.5, 2 (i.e. x is the number of moles of PVPA per moles of guanine unit in the polymer) were mixed. Rigid polymer membranes were obtained.

Doping was performed by dispersing the polymer in DMSO, then adding phosphoric acid with different ratios, x=0.5, 1, 1.5, 2 (i.e. x is the number of moles of acid per moles of guanine unit in the polymer). After evaporating the solvent, polymers were dried completely in a vacuum oven. Rigid polymer membranes were obtained.

3.2 SYNTHESIS OF THE IONICAL CROSS-LINKED POLYMER ELECTROLYTES

3.2.1 Chemicals

1-Vinyl-1,2,4-triazole (> 97%, Fluka), Vinylphosphonic acid (> 95%, Fluka) and DMF (> 99%, Fluka) were used as received. Azobisisobutyronitrile (AIBN; Merck) was recrystallized from THF. Polystyrene (M_n= 140 000 g mol^{-1}) was supplied by Aldrich. Phosphorus pentoxide, cyclohexane and sulfuric acid (98%) were purchased from Merck.

3.2.2 Synthesis of Poly (1-Vinyl-1,2,4-triazole) - Poly (vinyl phosponic acid)$_x$, PVTriP(VPA)$_x$

The PVTri, VTri was successfully produced via free-radical polymerization in toluene with a high yield (> 85%). Poly(vinyl phosphonic acid) was produced by free radical polymerization of vinyl phosphonic acid (Bingöl, 2006).

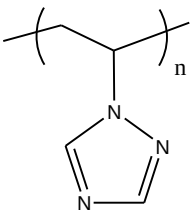

PVTri

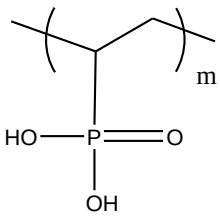

PVPA

Figure 3.4 Structure of PVTri and P(VPA)

A stoichiometric amounts of PVTri and PVPA solutions were dissolved to get PVTriP(VPA)$_{x}$; x=0.25, 0.5,1,2,4) where x is the molar ratio of the vinyl triazole (in PVTri) and vinylphosphonic acid (in PVPA) repeating units (Table 3.1). The complex polymer electrolytes were isolated in the solution as light yellowish gel. Then the solutions were further stirred under nitrogen atmosphere for 24 h, i.e., until getting a homogeneous milky solutions. The films were cast onto polished Poly(tetrafluoroethylene), PTFE plates and dried under vacuum at 50 ^{o}C and then stored in a glove box. After removal of the solvent, transparent, hygroscopic and free standing films were obtained and the samples denoted as PVTriP(VPA)$_{x}$ (Fig. 3.4).

Table 3.1 The proton conductivities and the glass transition temperatures (Tg) of the complex polymer electrolytes

Sample	Feed ratio (mol) VTri/VPA(x:y)	Relative Humidity (%)	Tg (^{o}C)	Max. Proton conductivity(S/cm)
PVTriP(VPA)	1-1	0	158	2.24x10^{-7} at 180 ^{o}C
PVTriP(VPA)$_2$	1-2	0	140	2.14x10^{-6} at 180^{o}C
PVTriP(VPA)$_2$	1-2	50	----	**0.022 at 100 ^{o}C**
PVTriP(VPA)$_4$	1-4	0	126	1.22x10^{-6} at 180 ^{o}C
PVTriP(VPA)$_4$	1-4	50	----	**0.008 at 100 ^{o}C**
PVTriP(VPA)$_{0.5}$	1-0.50	0	163	1.18x10^{-7} at 180 ^{o}C
PVTriP(VPA)$_{0.25}$	1-0.25	0	145	2.57x10^{-7} at 180 ^{o}C

3.2.3 Synthesis of Poly (1-Vinyl-1,2,4-triazole) - Poly (styrene sulfonic acid)$_x$, PVTriP(SSA)$_x$

The PVTri, VTri was successfully produced via free-radical polymerization in toluene with a high yield (> 85%). Poly(styrene sulfonic acid) was synthesized according to the procedure described in the literature (Ismail et al., 2005). Polystyrene was added into sulfuric acid/phosphorous pentoxide solution. The solution has been allowed to wait at 40 ºC for 1 h after stirring 30 min. Then, crushed ice has been added to the solution until PSSA completely precipitated out as a pale yellowish sticky bulk. Following, the precipitate was collected and dialyzed against water.

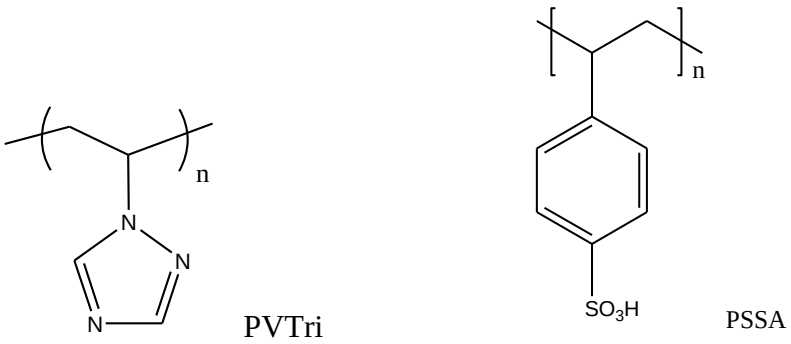

Figure 3.5 Structure of PVTri and P(SSA)

A stoichiometric amounts of PVTri and PSSA solutions were dissolved in water at several stoichiometric ratios x, which is the molar ratio of the vinyl triazole (in PVTri) to sulphonic acid (in PSSA) repeating units (Table 3.6). The complex polymer electrolytes were isolated in the solution as light yellowish gel. Then the solutions were further stirred under nitrogen atmosphere for 24 h, i.e., until getting a homogeneous milky solutions. The films were cast onto polished Poly(tetrafluoroethylene), PTFE

plates and dried under vacuum oven at 50 ^{o}C and then stored in a glove box. After removal of the solvent, transparent, hygroscopic and free standing films were obtained and the samples denoted as PVTriP(SSA)$_{x;}$ where x=0.25, 0.5,1,2,4) (Fig. 3.5).

Table 3.2 The proton conductivities and the glass transition temperatures (Tg) of the complex polymer electrolyte

Sample	Feed ratio (mol) VTri/SSA (x:y)	Tg (^{o}C)	Proton conductivity (S/cm)
PVTriPSSA	1-1	156	1,197 x 10^{-9} at 150 ^{o}C
PVTriPSSA$_2$	1-2	152	0.033 at 120 ^{o}C
PVTriPSSA$_4$	1-4	150	0.015 at 150 ^{o}C
PVTriPSSA$_{0.50}$	1-0.50	164	1,234 x 10^{-8} at 150 ^{o}C
PVTriPSSA$_{0.25}$	1-0.25	159	1,1 x 10^{-10} at 150 ^{o}C

3.3 Characterizations

3.3.1 FT-IR Spectroscopy

Fourier-Transform IR (FTIR) and ATR are most useful for identifying chemicals that are either organic or inorganic. This systems can be utilized to quantitate some components of an unknown mixture. They can be applied to the analysis of solids, liquids, and gasses. The term Fourier Transform Infrared Spectroscopy (FTIR) refer and ATR to a fairly recent development in the manner in which the data is collected and converted from an interference pattern to a spectrum. FTIR can be used to identify chemicals from spills, paints, polymers, coatings, drugs, and contaminants. FTIR is perhaps the most powerful tool for identifying types of chemical bonds (functional groups). The wavelength of light absorbed is characteristic of the chemical bond as can be seen in this annotated spectrum. The IR spectra (4000-400 cm^{-1}, resolution 4 cm^{-1}) were recorded with a Bruker Alpha-P in ATR-FTIR system. The spectra were analyzed to verify both azole functionalization of PGMA, PVTri and dopant interaction with azole units.

3.3.2 SEM Micrographs

The surface morphology of blend membranes was investigated by scanning electron microscopy (SEM, Philips XL30S-FEG). All of the samples were sputtered with gold for 150 s before SEM measurements.

3.3.3 Solid State ^{13}C CP-MAS NMR Measurements

Solid state ^{13}C CP-MAS NMR studies of the samples were performed using a Bruker Avance spectrometer at a Larmor frequency of 176.06 MHz in the Max-Planck Institute for Polymer Research, Mainz, Germany. All spectra were recorded with 1ms CP contact time, 15 kHz MAS frequency and 2 s relaxation delay time. ^{13}C CP-MAS NMR spectra of the samples were recorded at ~305 K.

3.3.4 ^{1}H MAS SQ and DQ NMR

^{1}H MAS NMR experiments on the samples were performed at a Bruker Avance spectrometer and by using a 2.5 mm fast MAS probe. All the ^{1}H experiments were performed at 25 kHz MAS frequency, to sufficiently suppress the homonuclear dipolar couplings of the dense proton-network. The 90^{o} pulse lengths were 2.5 μs. 2D DQ MAS experiments were performed using one-rotor period of the back-to-back (BABA) recoupling pulse sequence for the excitation and reconversion of dipolar ^{1}H-^{1}H DQ coherences.

3.3.5 Thermogravimetry (TG) Analysis

Thermogravimetry analysis (TGA) is based on the measurement of the weight loss of the material as a function of temperature, or isothermally as a function of time, in an atmosphere of nitrogen, helium, air, other gas, or in vacuum. TGA curve provides information concerning the thermal stability of the initial sample, intermediate compounds that may be formed and of the residue if any. In addition to thermal stability, the weight losses observed in TGA can be quantified to predict the pathway of

degradation or to obtain compositional information. The ability to vary atmosphere during the TGA evaluation, particularly from an inert to a reactive gas, provides additional information about a material composition and its stability. The experimental data offer more sophisticated understanding of reactions occurring at materials heating. Thermal stabilities of the all samples were examined by thermogravimetry (TG) analysis with a Perkin Elmer STA 6000. The samples (~ 10 mg) were heated from room temperature to 800 ^{o}C under N_2 and O_2 atmosphere at a scanning rate of 10 ^{o}C/min. The effect of dopant on thermal stability was determined using TG curves.

3.3.6 Differential Scanning Calorimetry (DSC) Analysis

DSC measures the temperatures and heat flow associated with transitions in materials as a function of time and temperature. It determines transition temperatures, melting and crystallization, and heat capacity. In heat flux insruments, the sample and reference are heated from the same source and the temperature difference is measured. In amorphous polymers DSC shows the glass transition temperature (T_g) and presence of single T_g verifies the homogeneity of the polymer. Differential scanning calorimetry (DSC) data were obtained using Perkin Elmer JADE DSC instrument The measurements were carried out at a rate of 10 ^{o}C min^{-1} under nitrogen atmosphere and heating-cooling curves were recorded at a rate of 10 ^{o}C/min. The glass transition temperatures were determined from the second heating curves and the effect of dopant on glass transition temperature was studied.

3.3.7 Proton Conductivity Measurements

The proton conductivity studies of the samples were performed using a SI 1260-Schlumberger impedance spectrometer. The conductivities were measured in the frequency range 1 Hz to 1 MHz at 10 ^{o}C intervals. The temperature was controlled with a Novocontrol cryosystem, which is applicable between -150 and 400 ^{o}C with a precision of 0.01 ^{o}C. The hot pressed pellets of the samples with a diameter of 10 mm and thickness of about 0.2-0.3 mm were sandwiched between two gold-coated electrodes (Fig. 3.7) and their conductivities were measured with 10 ^{o}C intervals under dry-nitrogen atmosphere.

3.3.8 Cyclic Voltammograms

Cyclic voltammograms were obtained with a potentiostat CHI instrument Model 842B. Voltammograms of PVTriP(SSA) were recorded in a three electrode CV system, using a polymer electrolyte modified Pt working electrode and a Pt counter electrode. The reference electrode was silver/silver chloride (Ag/AgCl) calibrated by a ferrocene/ferricinium redox system. Cyclic voltammetry studies were carried out in 0.1 M tetraethylammonium tetrafloroborate (TBATFB)/acetonitrile.

3.3.9 Water/Methanol Uptake

The solvent uptake measurements were made according to the literature (Li, 2004, Smitha, 2006). The pre-weighed dry films (Wdry) of the membranes were soaked into methanol/water (12 mol/L) solution. The external liquid of the swollen membranes was wiped out and they were weighted (Wwet) after different time intervals. The solvent uptake values were obtained using the following equation.

$$\text{Uptake}(\%) = (W_{wet}-W_{dry})/W_{dry} \times 100 \qquad (1)$$

CHAPTER 4

RESULTS AND DISCUSSION

4.1 ADENINE FUCTIONAL PGMA (PGMAAdenine) AND GUANINE FUNCTIONAL PGMA (PGMAGuanine)

4.1.1.1 FT-IR Studies

4.1.1.1 FT-IR Studies of PGMA, PGMAAdenine and Adenine

FT-IR spectra of PGMA, PGMAAdenine and Adenine are represented in Fig. 4.1. In PGMA the carbonyl group gives a strong peak at 1720 cm^{-1} and the strong peaks at 1140 cm^{-1} and 1260 cm^{-1} are attributed to C-O stretching of the ester group (Hirose et al., 2002). The absorption at 900 cm^{-1} is assigned to stretching vibration of the epoxy group which disappeared up on adenine functionalization. PGMAAdenine exhibited a medium absorption at 1577 cm^{-1} and 1450 cm^{-1} due to C=N and C-N stretching of the adenine molecule (A. Dkhissi et al. 2004). PGMAAdenine except a new absorption at 1640 cm^{-1} coming from amine bending vibration. PVPA shows strong bands at 1040-910 cm^{-1} that belong to asymmetric stretching vibrations of the P-OH group and at 1150 cm^{-1} that corresponds to P=O stretching (Bozkurt and Meyer, 2001). Additionally, phosphonic acid units give rise to broad bands with medium intensity at 1700-1590 cm^{-1} and 2850-2750 cm^{-1}.The broad band between 3500 cm^{-1} - 2500 cm^{-1} is the hydrogen bonding network which is necessary for proton conduction (Celik et al., 2008).

After doping PGMAAdenine with phosphoric acid the intensity of the peak at 1577 cm^{-1} decreases (A. Dkhissi et al. 2004). Additionally, the peak which appears at 3100 cm^{-1} shows the N-H absorption. Doping of PGMAAdenine with H_3PO_4, two strong peaks appear near 500 cm^{-1} and 1000 cm^{-1} which are attributed to PO_2 bending vibration of ($H_2PO_4^{2-}$) and P-O symmetric stretching of H_3PO_4 (Bouchet and Siebert, 1999). The carbonyl stretching band at 1725 cm^{-1} decreases and broadens due to protonation of C=O bond. Similar absorption bands are also present in FT-IR spectra of PGMAAdenine except a new absorption at 1650 cm^{-1} coming from amine bending vibration.

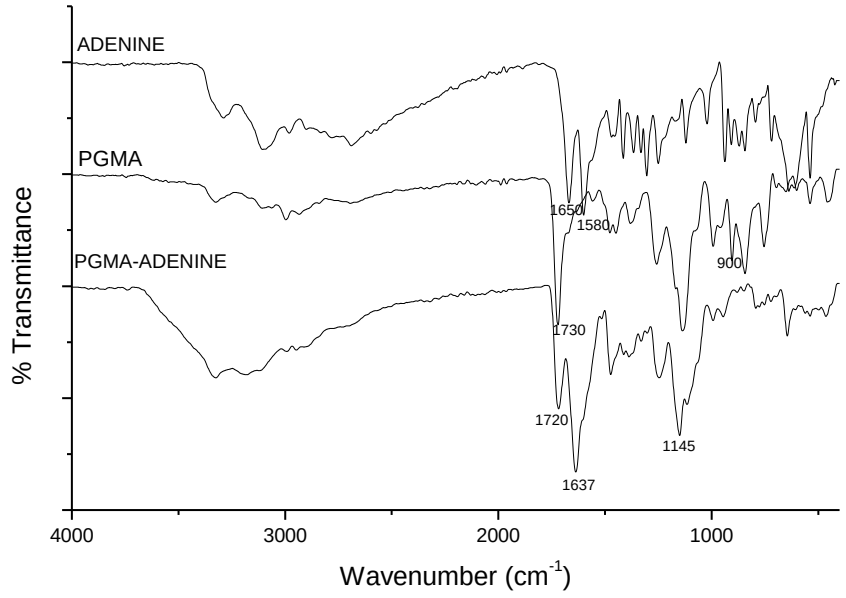

Figure 4.1 FT-IR spectra of PGMA, PGMAAdenine and Adenine.

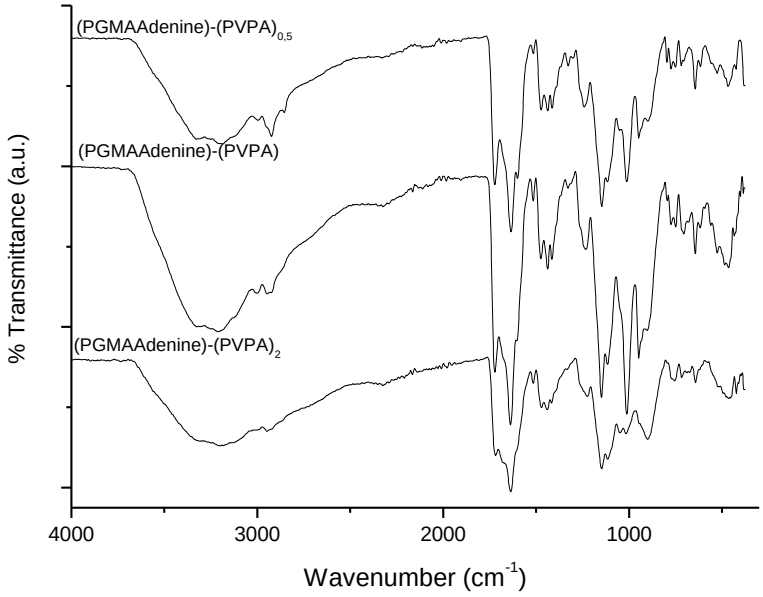

Figure 4.2 FT-IR spectra of PVPA blends of PGMAAdenine.

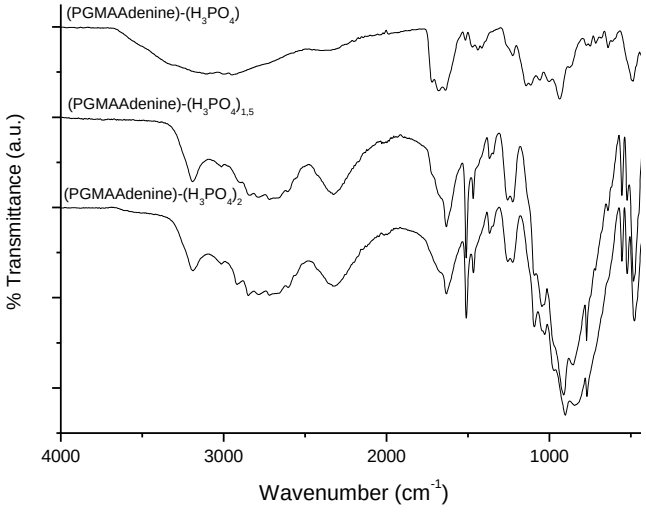

Figure 4.3 FT-IR spectra of H_3PO_4 doped PGMAAdenine.

4.1.1.2 FT-IR Studies of PGMA, PGMAGuanine and Guanine

FT-IR spectra of PGMA, PGMAGuanine and guanine are represented in Fig. 4.4. In PGMA the carbonyl group gives a strong peak at 1720 cm^{-1} and the strong peaks at 1140 cm^{-1} and 1260 cm^{-1} are attributed to C-O stretching of the ester group (Hirose et al., 2002). The absorption at 900 cm^{-1} is assigned to stretching vibration of the epoxy group which disappeared up on adenine functionalization. Guanine exhibited a medium absorption at 1650 cm^{-1} and 1550 cm^{-1} due to amine bond. The epoxy absorption peak at 900 cm^{-1} disappeared up on guanine functionalization. Additionally, phosphonic acid units give rise to broad bands with medium intensity at 1700-1590 cm^{-1} and 2850-2750 cm^{-1}.The broad band between 3500 cm^{-1} - 2500 cm^{-1} is the hydrogen bonding network which is necessary for proton conduction (Celik et al., 2008). After doping the PGMAGuanine with H_3PO_4, two strong peaks appear near 500 cm^{-1} and 1000 cm^{-1} which are attributed to PO_2 bending vibration of ($H_2PO_4^{2-}$) and P-O symmetric stretching of H_3PO_4 (Bouchet and Siebert, 1999). The carbonyl stretching band at 1715 cm^{-1} broadens due to protonation.

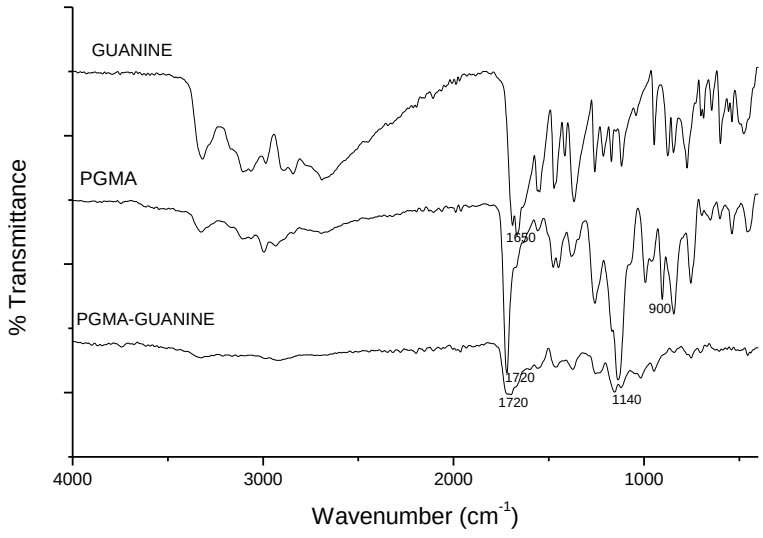

Figure 4.4 FT-IR spectra of PGMA, PGMAGuanine and Guanine.

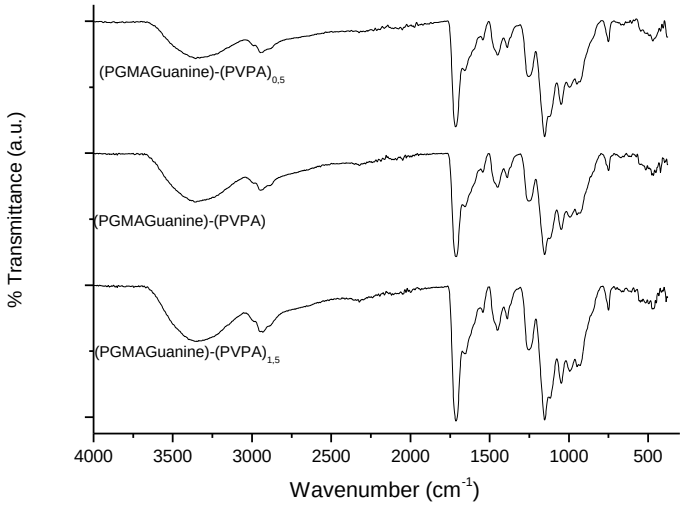

Figure 4.5 FT-IR spectra of PVPA blends of PGMAGuanine.

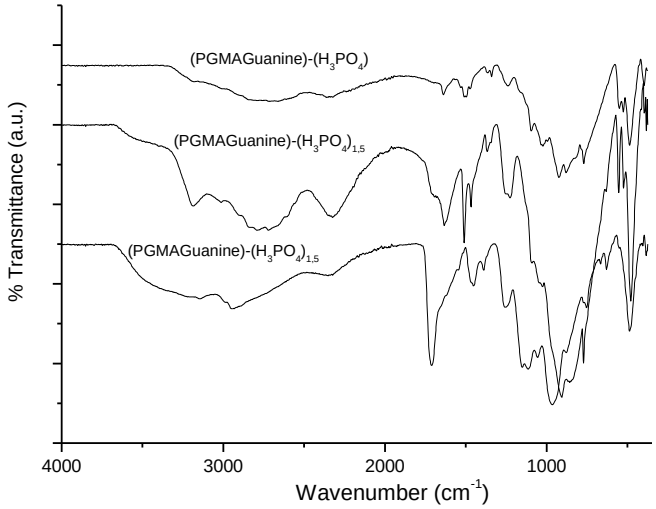

Figure 4.6 FT-IR spectra of PGMA, PGMAGuanine and Guanine.

4.1.2 Solid State ^{13}C CP-MAS NMR Results

4.1.2.1 Solid State ^{13}C CP-MAS NMR Spectra of PGMAAdenine

The solid state ^{13}C CP-MAS NMR spectra of PGMAAdenine is shown in Fig. 4.7 respectively. The characteristic C peaks of the adenine are between 140-160 ppm and the peak located at around 180 ppm belongs to C of the carbonyl group. Signals corresponding to the methyl and methylene groups appear between 15-75 ppm. Resonances are similar for both samples, except those in the 120-170 ppm region. This difference in the Adenine functional polymer may originate from the polymerization procedure, where the additional NH sites in the adenine may result in some side reactions leading to inter and/or intra chain cross-linking.

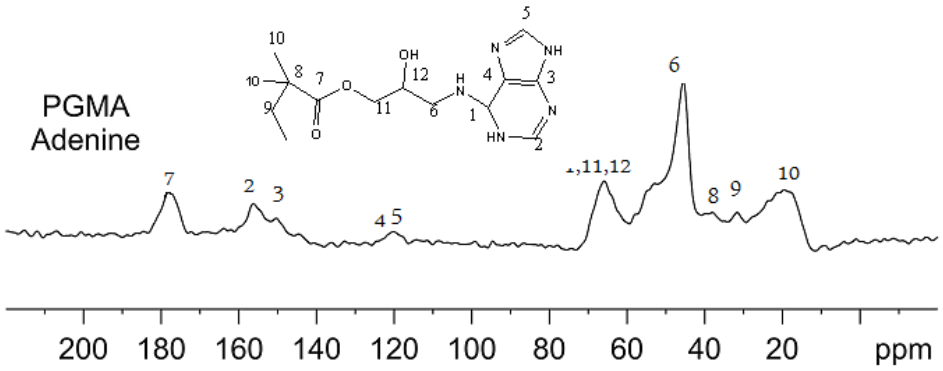

Figure 4.7 The solid state ^{13}C CP-MAS NMR spectrum of PGMAAdenine.

4.1.2.2 Solid State ^{13}C CP-MAS NMR Spectra of PGMAGuanine

The solid state ^{13}C CP-MAS NMR spectra of PGMAGuanine is shown in Fig. 4.8. The characteristic C peak of the guanine is between 150-170 ppm and the peak located at around 180 ppm belongs to C of the carbonyl group. Signals corresponding to the methyl and methylene groups appear between 15-75 ppm.

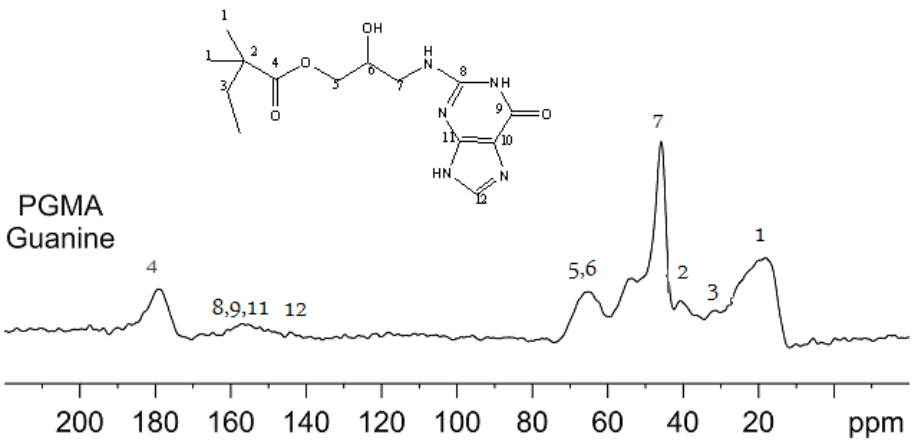

Figure 4.8 The solid state ^{13}C CP-MAS NMR spectrum of PGMAGuanine.

4.1.3 ^{1}H MAS SQ and DQ NMR

4.1.3.1 ^{1}H MAS SQ and DQ NMR of PGMAAdenine and PGMAGuanine

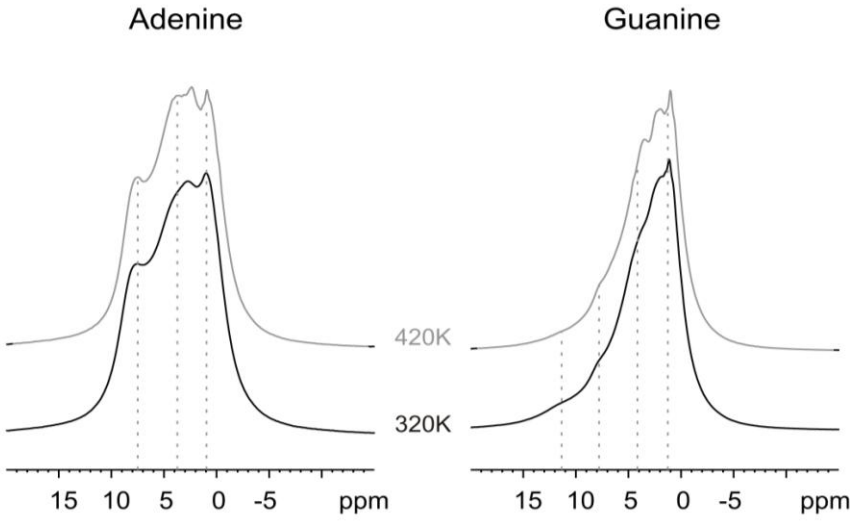

Figure 4.9 ^{1}H MAS NMR spectra of adenine and guanine functional PGMA polymer.

From Fig. 4.9, different proton sites in the studied materials can be identified. The aliphatic, aromatic and hydrogen-bonded acidic protons are observed at different spectral positions. No indication of strong hydrogen bonding is observed for adenine functional

polymer, since there is no high chemical shift proton resonance in the spectrum. Guanine functional polymer, however, has a broad resonance at ~12 ppm, which indicates the presence of hydrogen bonding. The resonance is not well resolved, and relatively broad. This observation indicates the lack of molecular mobility in the system, which is observed in all of the 1H spectra at low temperature and even at high temperature. This also manifests itself in the observed proton conductivity values, which are relatively small, compared to other studied materials having phosphoric acid or azole derivatives (Bozkurt et al., 2008, Akbey et al., 2009).

The spectra recorded at 420 K, have slightly narrower lines. However, still the molecular mobility is not much to result in the removal of any resonance from the ^{1}H spectra after the application of double-quantum filtration.

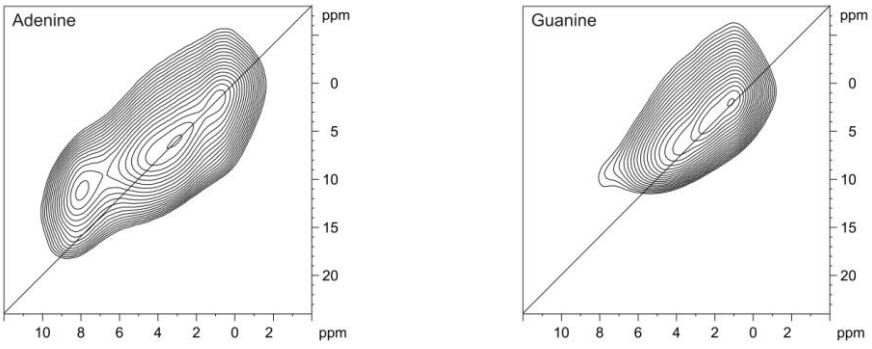

Figure 4.10 2D ^{1}H DQ MAS NMR spectra of adenine and guanine functional PGMA polymer.

Fig. 4.10 represents the 2D ^{1}H DQ MAS NMR spectra recorded at 320 K and 25 kHz MAS. The spectra show explicitly the proton proximities less than 4.5 Å in the polymer materials. Aliphatic-aliphatic and aliphatic-aromatic proton cross-peaks are present. Additionally, several auto-peaks which are on the diagonal line are observed showing the proximities of same type of protons to each other.

An interesting observation is the absence of the hydrogen-bonded proton auto peak in any of the spectra. This is indicating that the hydrogen bonded protons are not close in space to each other. Moreover, the lack of cross peaks to other types of the protons indicate that the hydrogen-bonded proton is either isolated, or relatively mobile and not represent and dipolar

coupling to other proton species. The latter is not likely, since the double-quantum filtration did not result in any signal loss for those sites. As a result, is can be said that the hydrogen-bonded protons are relatively apart from each other and from other protons due to whatever organization of the aromatic sites.

4.1.4 SEM Micrographs

4.1.4.1 SEM Micrographs of PGMAAdenine

Surface morphologies (PGMAAdenine)-(PVPA) membranes at different magnifications were investigated by scanning electron microscopy (Fig. 4.11a and Fig. 4.11b). Due to strong interaction between of phosfonic acid groups of PVPA and the adenine units of PGMAAdenine, no phase separation occurred during solvent evaporation, hence homogeneous and transparent films formed. This result is also consistent with the DSC curves of the membranes that no separate T_g transition of impregnated PVPA was observed.

(a) **(b)**

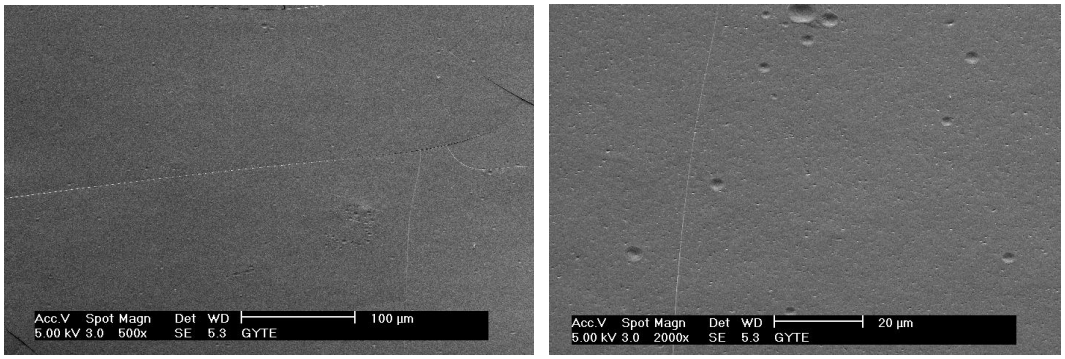

Figure 4.11 SEM micrographs of the surface of (PGMAAdenine)-(PVPA) (a) 100 μm (b) 20 μm.

4.1.4.2 SEM Micrographs of PGMAGuanine

Surface morphologies (PGMAGuanine)-(PVPA) membranes at different magnifications were investigated by scanning electron microscopy (Fig. 4.12a and Fig. 4.12b). Due to strong interaction between of phosfonic acid groups of PVPA and the guanine units of PGMAGuanine, no phase separation occurred during solvent evaporation, hence homogeneous and transparent films formed. This result is also consistent with the DSC curves of the membranes that no separate T_g transition of impregnated PVPA was observed.

(a) **(b)**

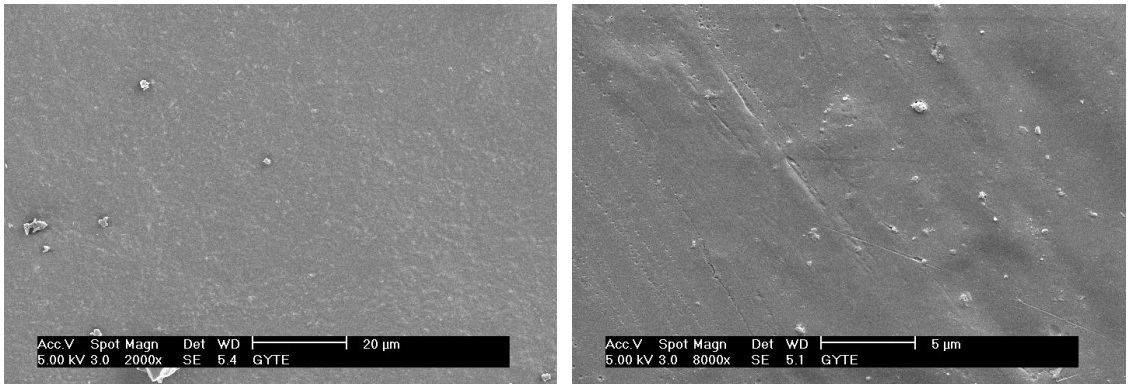

Figure 4.12 SEM micrographs of the surface of (PGMAGuanine)-(PVPA) (a) 20 μm (b) 5 μm.

4.1.5 Elemental Analysis

Adenine and Guanine immobilizations is very important for this study and elemental analysis is used to verify this reaction. The backbone of PGMA does not contain nitrogen so the nitrogen contribution into the functional polymers comes from the adenine and guanine units. Nitrogen contents of the samples were used to calculate adenine and guanine ratio of the functional polymers. As seen in Table 6.1 more than 80 % of the epoxide rings were

opened by adenine units and more than 50 % of the epoxide ring were opened by guanine units.

Table 4.1 Azole contents of the polymers calculated by Elemental Analysis results.

	PGMAGuanine	PGMAAdenine
N %	9.37	16.22
C %	70.70	47.31
H %	7.89	4.90

4.1.6 Thermogravimetry (Tg) Analysis of PGMAAdenine and PGMAGuanine

4.1.6.1 Tg of PGMAAdenine

It was reported that the weight loss in PGMA occurs in two steps within 200-400 ^{o}C (Nanjundan et al., 2005). Fig. 4.13 and 4.14 show the thermograms of PVPA blends and H_3PO_4 doped PGMAAdenine samples. The slight weight change until 100-150 ^{o}C can be attributed to absorbed humidity. Clearly, PGMAAdenine is thermally stable up to at least 250 ^{o}C. After 250^{o}C a remarkable weight loss derives from the thermal decomposition of the polymer main chain. In (PGMAAdenine)-$(PVPA)_x$, the stepwise decomposition after 200 ^{o}C, can be attributed to water liberation due to the self-condensation of the phosphonic acid and also decomposition the polymer main chain contributes to further weight loss.

TG profiles of H_3PO_4 doped (PGMAAdenine) illustrate no weight change up to approximately 180 ^{o}C. After 200 ^{o}C, can be attributed to water liberation due to the self-condensation of the phosphoric acid and also decomposition the polymer main chain contributes to further weight loss. Clearly, (PGMAAdenine)-$(H_3PO_4)_x$ the materials are thermally stable up to 200 ^{o}C and then they decompose.

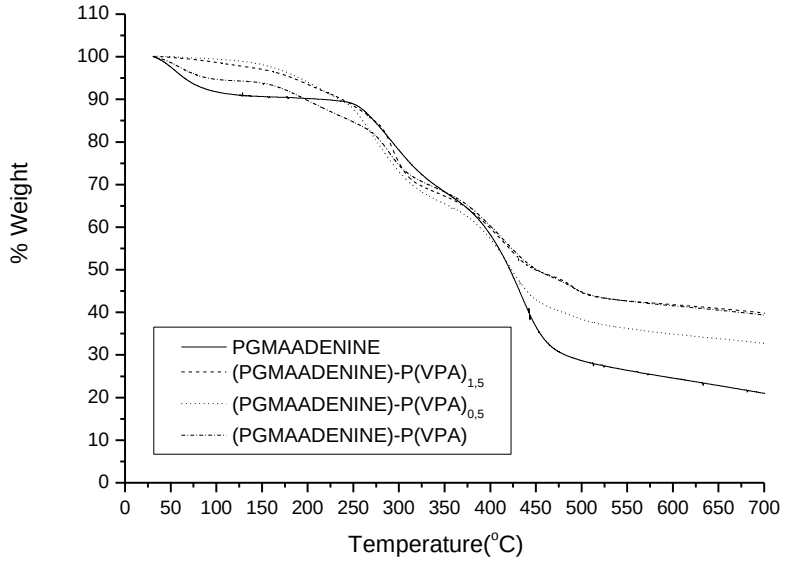

Figure 4.13 Tg profiles of PGMAAdenine, (PGMAAdenine)-(PVPA), (PGMAAdenine)-$(PVPA)_{0,5}$, and (PGMAAdenine)-$(PVPA)_{1,5}$, under a N_2 atmosphere at a heating rate of 10 ^{0}C/min.

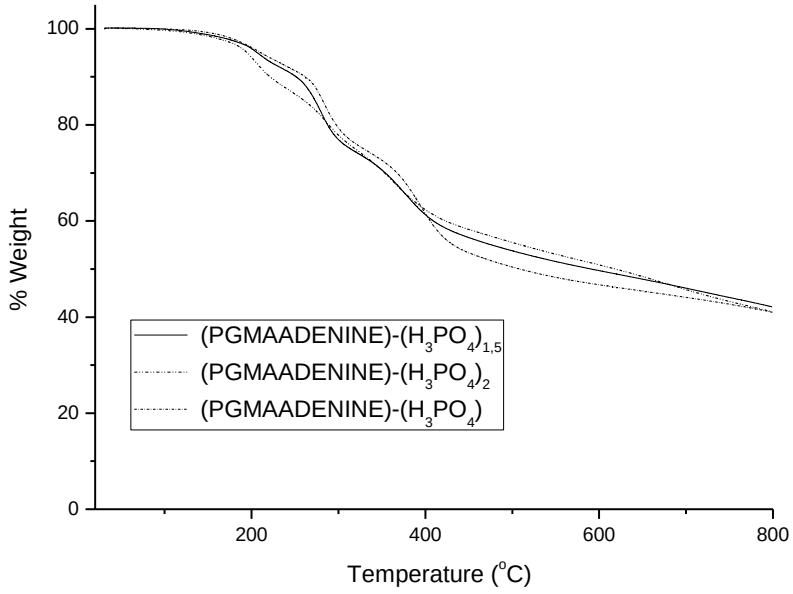

Figure 4.14 Tg profiles of H_3PO_4 doped (PGMAAdenine) under a N_2 atmosphere at a heating rate of 10 ^{0}C/min.

4.1.6.2 Tg of PGMAGuanine

The decomposition of PGMA was reported to occur in two steps with in 200-400 ^{o}C (Nanjundan et al., 2005). Fig. 4.15 and 4.16 show the thermograms of the PVPA blends of functional polymer (PGMAGuanine)-$(PVPA)_x$ and doped sample, (PGMAGuanine)-$(H_3PO_4)_x$. Clearly, PGMAGuanine is thermally stable up to at least 230 ^{o}C For the (PGMAGuanine)-$(PVPA)_x$, an elusive weight change until 180 ^{o}C may be attributed to the loss of absorbed humidity then degradation of the polymer main chain and the functional units starts.

The doped samples exhibit an insignificant weight change until 180 ^{o}C. The stepwise decomposition above this temperature can be attributed to water liberation due to the self-condensation of the phosphoric acid as well as the decomposition of the polymer.

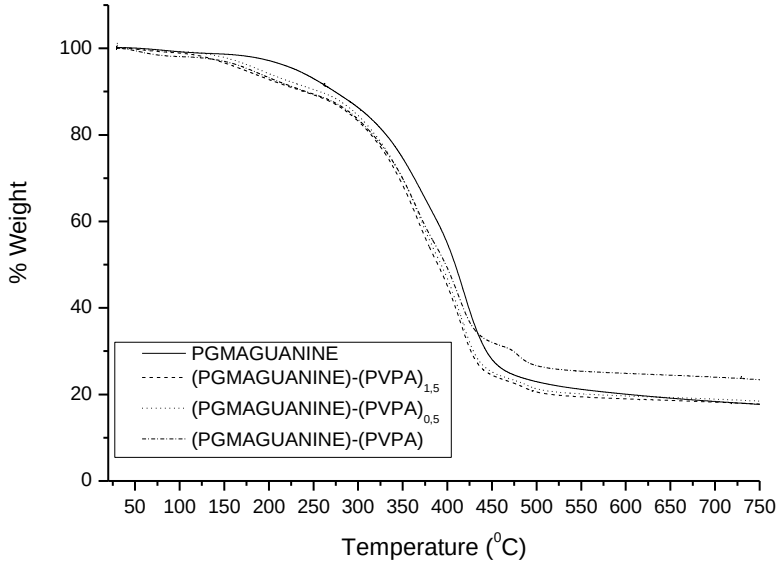

Figure 4.15 Tg profiles of PGMAGuanine, (PGMAGuanine)-(PVPA), (PGMAGuanine)-$(PVPA)_{0,5}$, and (PGMAGuanine)-$(PVPA)_{1,5}$, under a N_2 atmosphere at a heating rate of 10 ^{0}C/min.

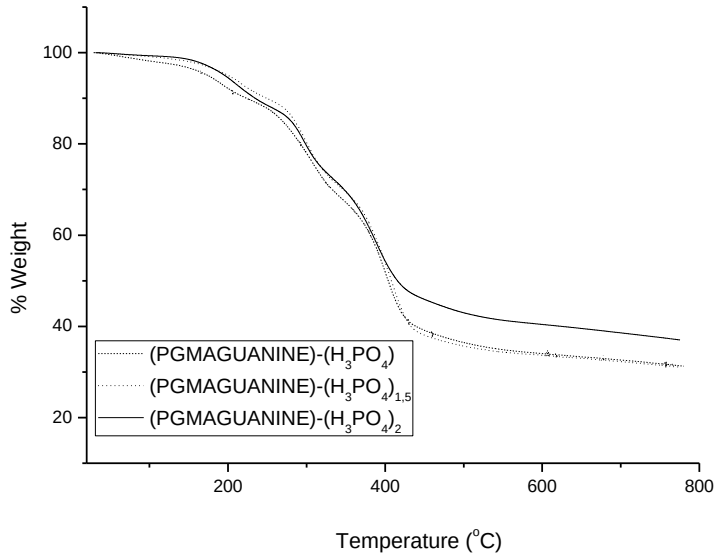

Figure 4.16 Tg profiles of H_3PO_4 doped (PGMAGuanine) under a N_2 atmosphere at a heating rate of 10 ^{0}C/min.

4.1.7 DSC Measurements of PGMAAdenine and PGMAGuanine

4.1.7.1 DSC of PGMAAdenine

The glass transition temperatures (T_g) of the homopolymer (PGMA) was reported to be about 74 ^{o}C (Nanjundan et al., 2005). Fig. 4.17 shows DSC thermograms of PVPA blends of PGMAAdenine. The T_g of PGMAAdenine is 161 ^{o}C, (PGMAAdenine)-(PVPA) is 173 ^{o}C and that of (PGMAAdenine)-$(PVPA)_{1,5}$ is 192 ^{o}C. The results demonstrated that as the quantity of PVPA increased, the glass transition temperature of the samples shifted to higher temperatures. The T_g for PGMAAdenine (161 ^{o}C) shifted to +31 ^{o}C for (PGMAAdenine)-$(PVPA)_{1,5}$. The presence of single glass transition shows the homogeneity of the materials.

Fig. 4.18 shows DSC thermograms of H_3PO_4 doped PGMAAdenine. The T_g of PGMAAdenine exhibits a glass transition at around 161 ^{o}C and the Tg shifts to 106, 175 and 113 ^{o}C for (PGMAAdenine)-(H_3PO_4), (PGMAAdenine)-$(H_3PO_4)_{1,5}$ and (PGMAAdenine)-$(H_3PO_4)_2$ respectively. The presence of single Tg confirms the homogeneity of the doped samples.

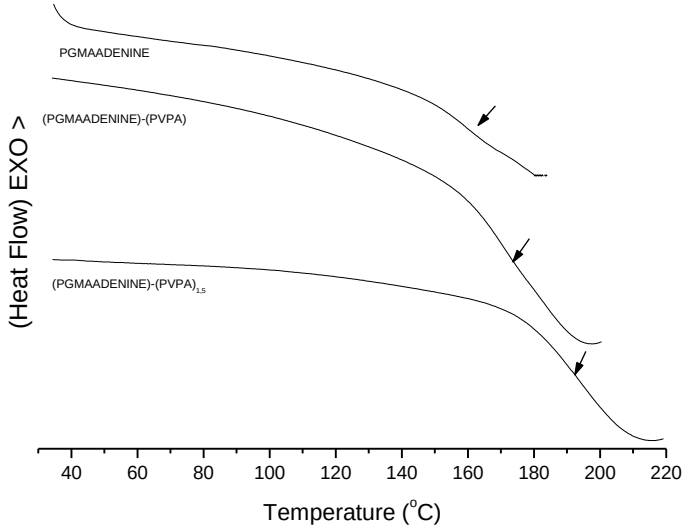

Figure 4.17 DSC traces of PGMAAdenine, (PGMAAdenine)-(PVPA) and (PGMAAdenine)- $(PVPA)_{1,5}$, under a N_2 atmosphere at a heating rate of 10 ^{0}C/min.

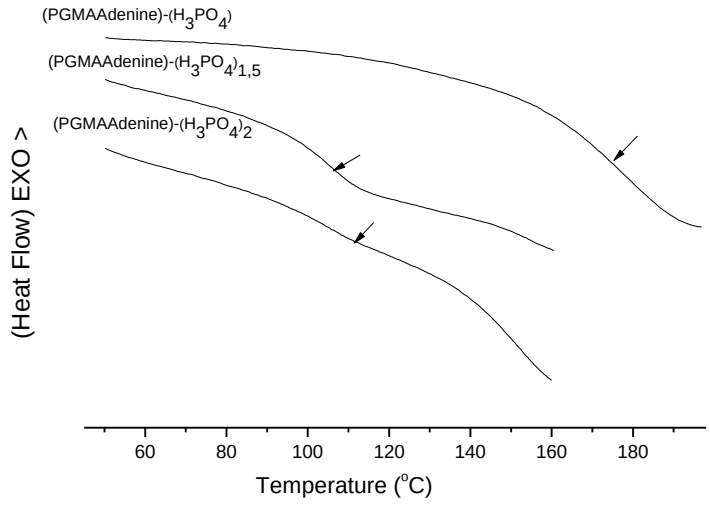

Figure 4.18 DSC traces of (PGMAAdenine)-(H_3PO_4), (PGMAAdenine)-$(H_3PO_4)_{1,5}$, and (PGMAAdenine)-$(H_3PO_4)_2$ under a N_2 atmosphere at a heating rate of 10 ^{0}C/min.

4.1.7.2 DSC of PGMAGuanine

,

Fig. 4.19 shows the DSC thermograms of PVPA functional PGMAGuanine. The glass transition temperature of T_g of the homopolymer PGMA was reported to be near 74 ^oC (Nanjundan et al., 2005). While the PGMAGuanine has a T_g of 192 ^oC. The Tg of (PGMAGuanine)-(PVPA) which was found to be 161 ^oC, shifted to 31 ^oC for (PGMAGuanine)-(PVPA). The (PGMAGuanine)-$(PVPA)_{1,5}$ has a T_g of 176 ^oC. The presence of single glass transition shows the homogeneity of the materials.

Fig. 4.20 shows DSC thermograms of H_3PO_4 doped PGMAGuanine. The T_g of PGMAGuanine exhibits a glass transition at around 192 ^oC and the Tg shifts to 156, 108 and 111 ^oC for (PGMAGuanine)-(H_3PO_4), (PGMAGuanine)-$(H_3PO_4)_{1,5}$ and (PGMAGuanine)-$(H_3PO_4)_2$ respectively. The presence of single Tg confirms the homogeneity of the doped samples.

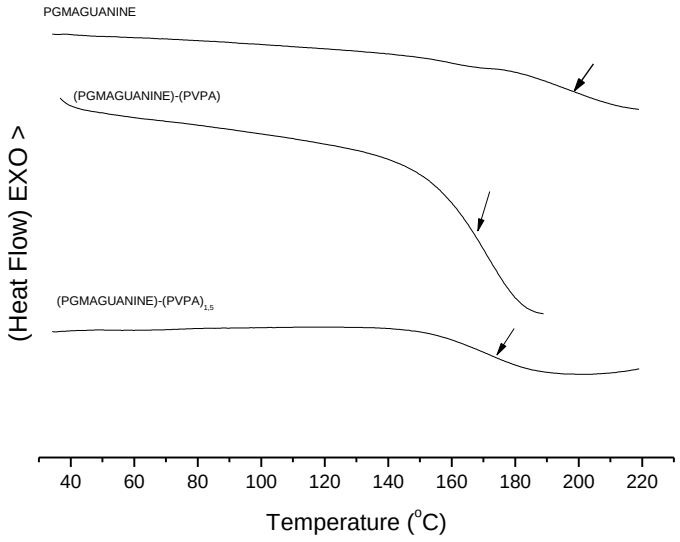

Figure 4.19 DSC traces of PGMAGuanine, (PGMAGuanine)- (PVPA) and (PGMAGuanine)-$(PVPA)_{1,5}$, under a N_2 atmosphere at a heating rate of 10 ^0C/min.

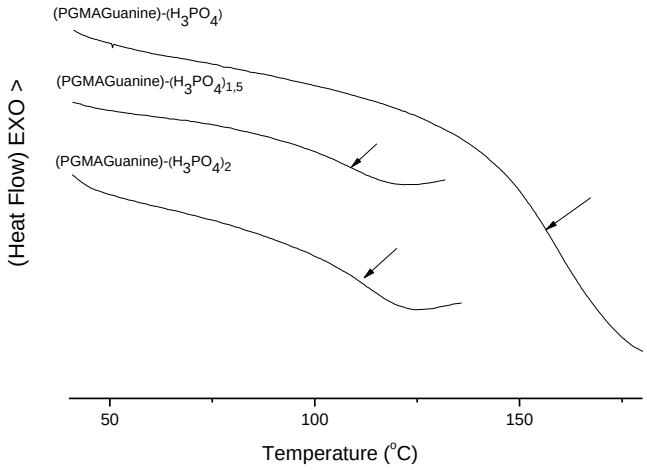

Figure 4.20 DSC traces of (PGMAGuanine)-(H_3PO_4), (PGMAGuanine)-$(H_3PO_4)_{1,5}$ and (PGMAGuanine)-$(H_3PO_4)_2$ under a N_2 atmosphere at a heating rate of 10 ^{0}C/min.

4.1.7 Proton Conductivity Studies

4.1.8.1 AC Conductivity Measurements

The AC conductivities, σ_{ac} (ω) of the polymers were measured at several temperatures using impedance spectroscopy. Frequency dependent AC conductivities (σ_{ac} (ω)) were measured using Eq. 1;

$$\sigma'(\omega) = \sigma_{ac}(\omega) = \varepsilon''(\omega)\,\omega\,\varepsilon_o \qquad (1)$$

where $\sigma'(\omega)$ is the real part of conductivity, $\omega = 2\pi f$ is the angular frequency, ε_o is the vacuum permittivity (ε_o = 8.852 x 10^{-14} F/cm), and ε'' is the imaginary part of complex dielectric permittivity (ε^*).

4.1.8.2 DC Conductivity Measurements

The DC conductivity, σ_{dc} is derived from the log scale σ_{ac} versus F curves by linear fitting plateau regions and extrapolating to zero frequency. If the system exhibits Arrhenius behavior, the conductivity isotherm can be fitted by Arrhenius equation (Eq. 2);

$$\ln \sigma = \ln\sigma_o - E_a/kT \quad (2)$$

where σ_o is the pre-exponential terms, E_a is the activation energy, and k is the Boltzmann constant. If the system follows VTF behavior the curved DC conductivity isotherm can be fitted by Vogel-Tamman–Fulcher-type (VTF) equation (Eq. 3);

$$\log \sigma = \log \sigma_o - E_v/[k(T-T_o)] \quad (3)$$

where σ_o is the conductivity at infinite temperature, E_v is the Vogel activation energy and T_o is the Vogel temperature.

4.1.8.3 Conductivity of pure and doped PGMAAdenine

The AC and DC conductivities of pure and doped triazole functional polymers are shown in Fig. 4.21–4.27. All samples exhibit higher conductivities at high temperature. Pure polymers do not exhibit considerable proton conductivity even at high temperatures ($<10^{-6}$). In addition, there is no significant proton conductivity of PVPA functional polymers in the anhydrous state. The reason can be the aggregation adenine units in the host polymer which may inhibit continuous defect type conduction. H_3PO_4 doped PGMAAdenine systems have higher conductivity than PVPA blends of PGMAAdenine systems.

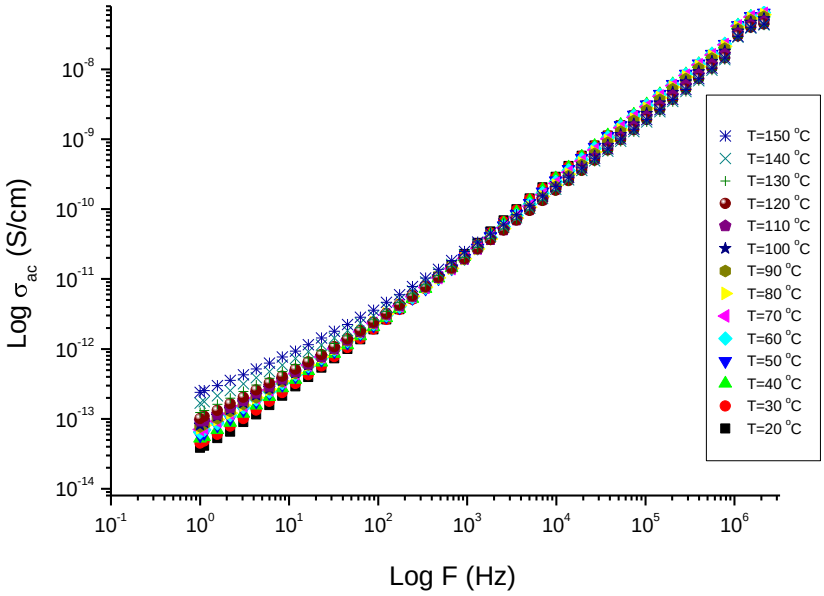

Figure 4.21 AC conductivity versus Frequency (Hz) for PGMAdenine at various temperatures.

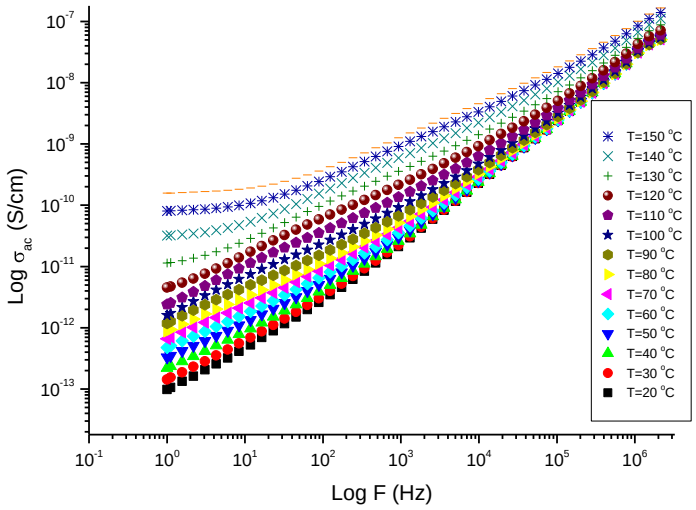

Figure 4.22 AC conductivity versus Frequency (Hz) for (PGMAAdenine)-(PVPA) at various temperatures.

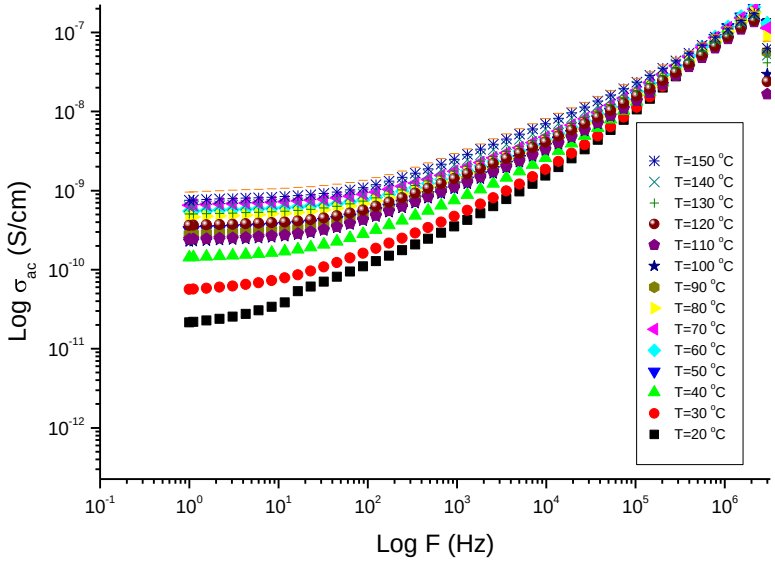

Figure 4.23 AC conductivity versus Frequency (Hz) for (PGMAAdenine)-$(PVPA)_{1,5}$ at various temperatures.

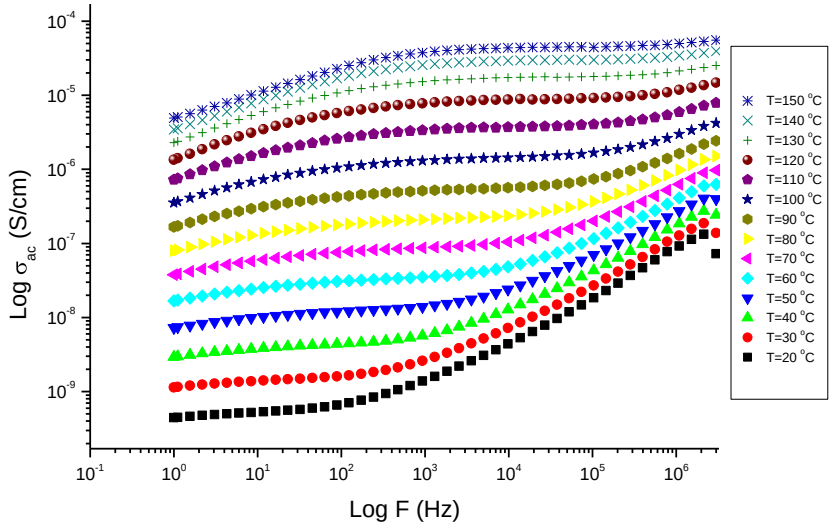

Figure 4.24 AC conductivity versus Frequency (Hz) for (PGMAAdenine)-$(H_3PO_4)_{1,5}$ at various temperatures.

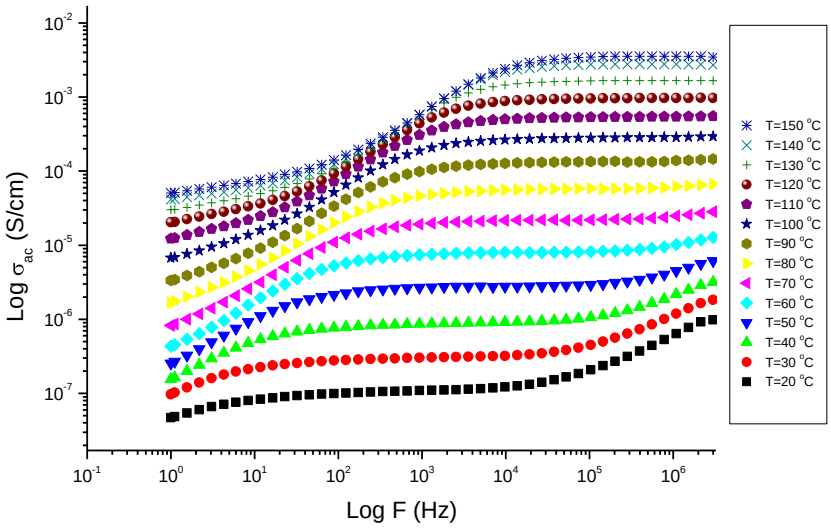

Figure 4.25 AC conductivity versus Frequency (Hz) for (PGMAAdenine)-$(H_3PO_4)_2$ at various temperatures.

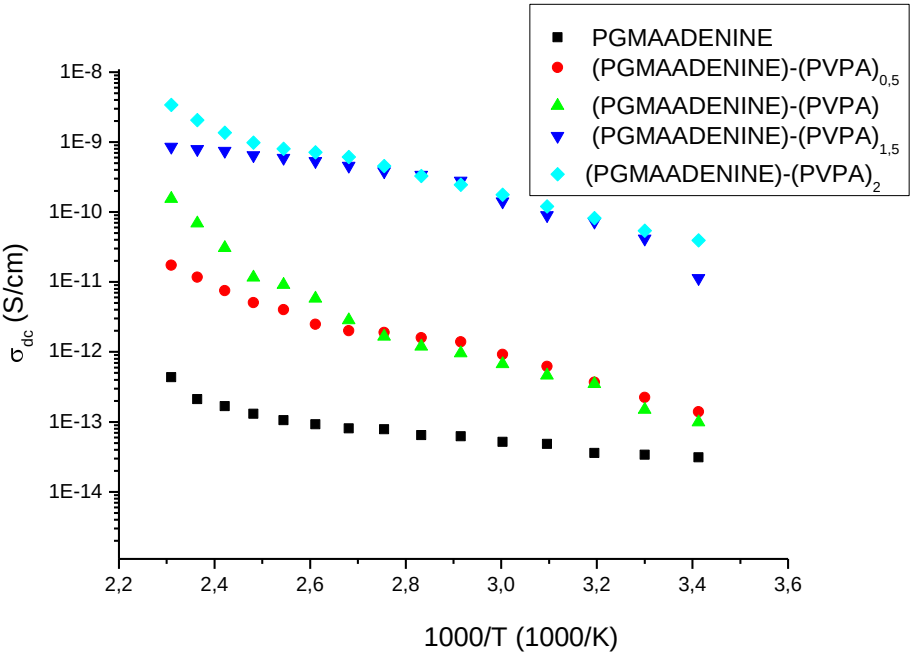

Figure 4.26 DC conductivities of PGMAAdenine, (PGMAAdenine)- $(PVPA)_{0,5}$, (PGMAAdenine)-(PVPA), (PGMAAdenine)-$(PVPA)_{1,5}$ and (PGMAAdenine)-$(PVPA)_2$ as a function of reciprocal temperature.

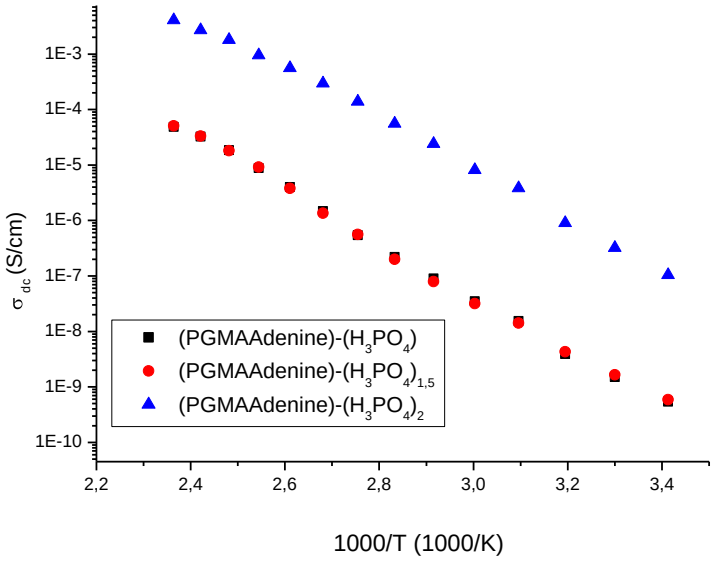

Figure 4.27 DC conductivities of (PGMAAdenine)-(H_3PO_4), (PGMAAdenine)-$(H_3PO_4)_{1,5}$, and (PGMAAdenine)-$(H_3PO_4)_2$ as a function of reciprocal temperature.

Among phosphoric acid doped systems, (PGMAAdenine)-$(H_3PO_4)_2$ showed the highest proton conductivity of ~0.004 S/cm at 150 ^oC in the anhydrous state.

Normally, there are two different transport mechanisms that contribute to the proton conductivity in phosphoric acid-doped polymersystems. The first is the structural diffusion (Grotthuss mechanism) in which the conductivity is mainly controlled by proton transport through phosphate ions, i.e. $H_4PO_4^+$, $H_2PO_4^-$ (Grotthuss proton transport). The second is the vehicle mechanism where the protons travel through the material on a neutral or charged "vehicle". Several studies were reported about the contribution of these mechanisms on the proton conductivity of pure phosphoric acid and it was indicated that the former is much more predominant and the conduction mechanism is mainly controlled by the structural diffusion rather than vehicle mechanism. In the current system, the presence of HPO_4^{2-} and $H_2PO_4^-$ anions implies that the proton diffusion can also occur throughout these ionized species.

It seems that the proton hopping from one N–H site to a free nitrogen contributes to the conductivity of (PGMAAdenine)-$(H_3PO_4)_x$ systems as in the case of imidazole where the

long range proton transfer occurs throughout the protonic defects, i.e., protons transport between protonated and unprotonated heterocyclic units. In addition, proton hopping from one N–H site to phosphate ions may also contribute to the conductivity.

4.1.8.4 Conductivity of pure and doped PGMAGuanine

The AC conductivities of phosphoric acid doped PGMAGuanine and PVPA blends of PGMAGuanine are shown in Fig. 4.28-4.34. All samples exhibit higher conductivities at high temperature.

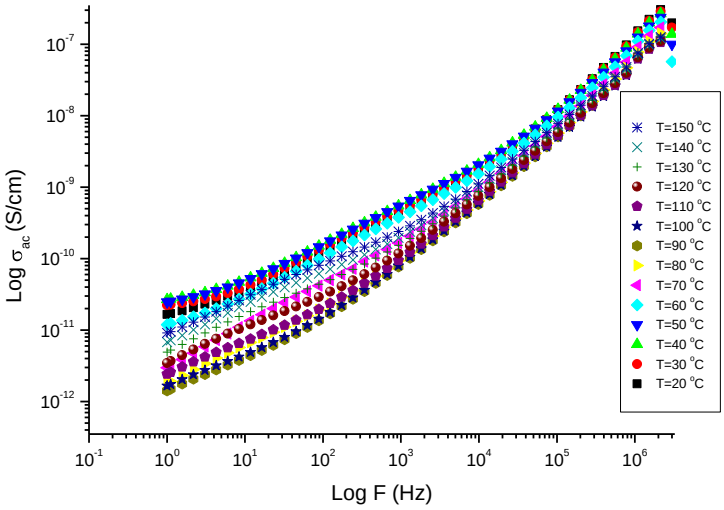

Figure 4.28 AC conductivity versus Frequency (Hz) for PGMAGuanine at various temperatures.

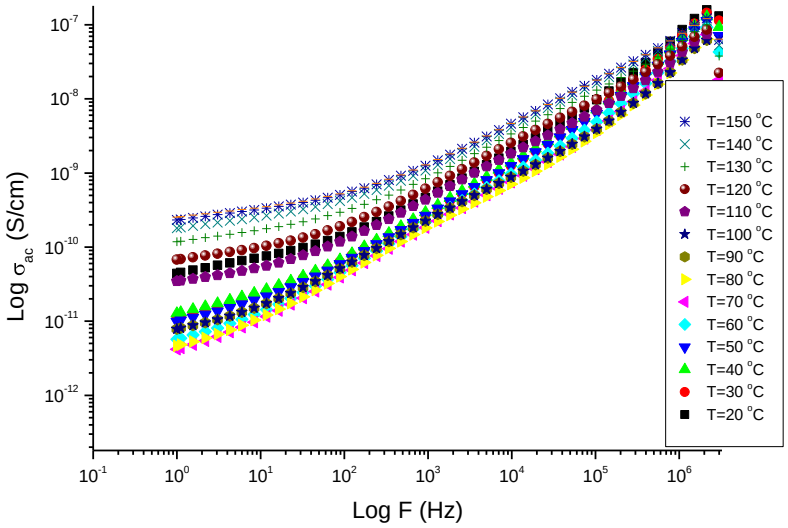

Figure 4.29 AC conductivity versus Frequency (Hz) for (PGMAGuanine)-(PVPA) at various temperatures.

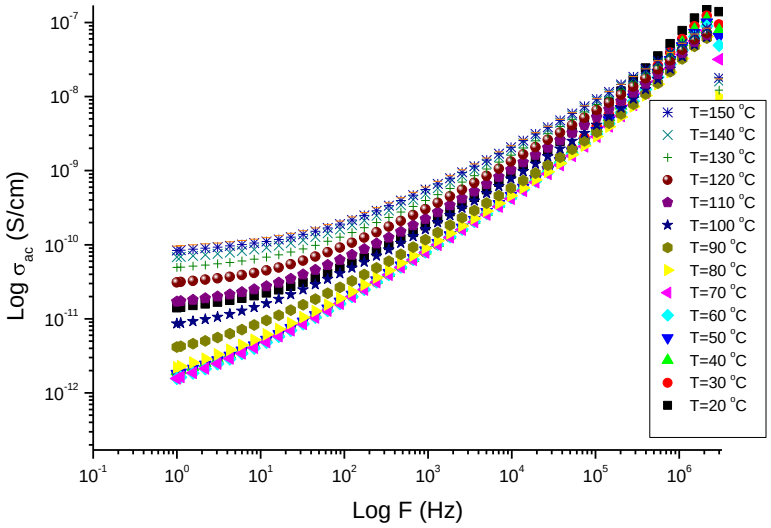

Figure 4.30 AC conductivity versus Frequency (Hz) for (PGMAGuanine)-$(PVPA)_{1,5}$ at various temperatures.

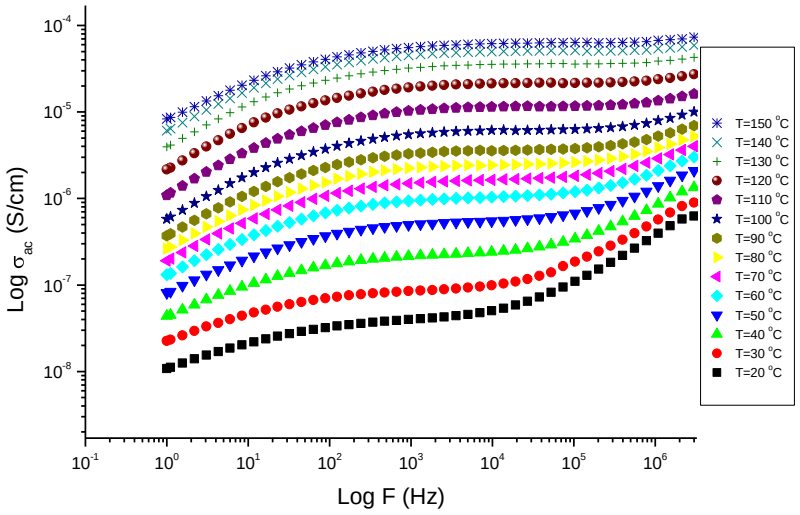

Figure 4.31 AC conductivity versus Frequency (Hz) for (PGMAGuanine)-$(H_3PO_4)_{1,5}$ at various temperatures.

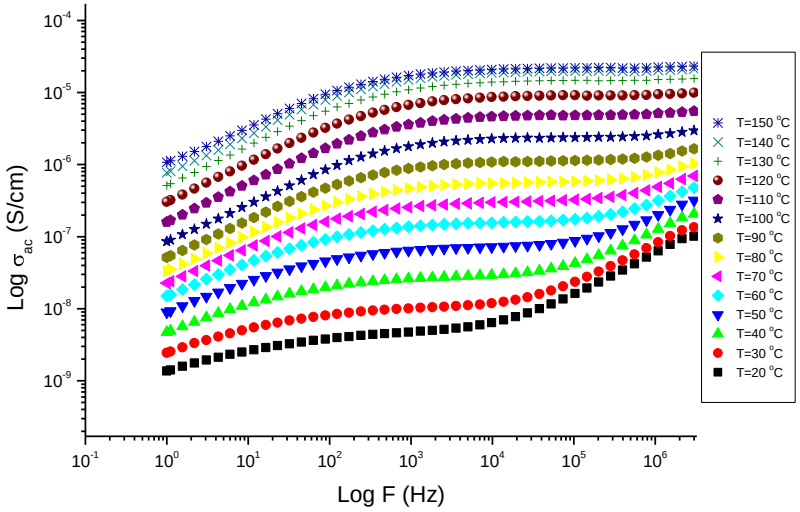

Figure 4.32 AC conductivity versus Frequency (Hz) for (PGMAGuanine) - $(H_3PO_4)_2$ at various temperatures.

The DC conductivities of PGMAGuanine samples were compared in Fig. 4.25 and 4.26 to determine the effect of PVPA and H_3PO_4 on proton conductivity. Fig. 4.25 and 4.26 indicates that the conductivity strongly depends on temperature and the phosphonic acid -

phosphoric acid content. Generally, phosphonic acid - phosphoric acid doped systems exhibit Arrhenius behavior at all samples.

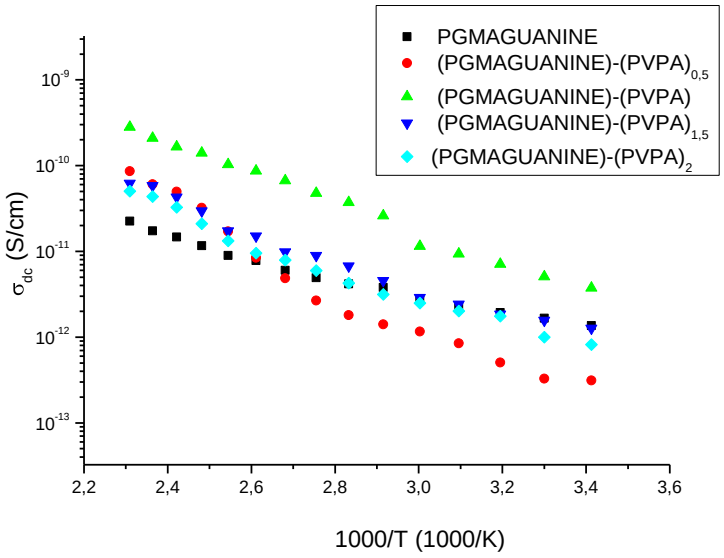

Figure 4.33 DC conductivities of PGMAGuanine, (PGMAGuanine)-(PVPA), (PGMAGuanine)-$(PVPA)_{1,5}$ and (PGMAGuanine)-$(PVPA)_2$ as a function of reciprocal temperature.

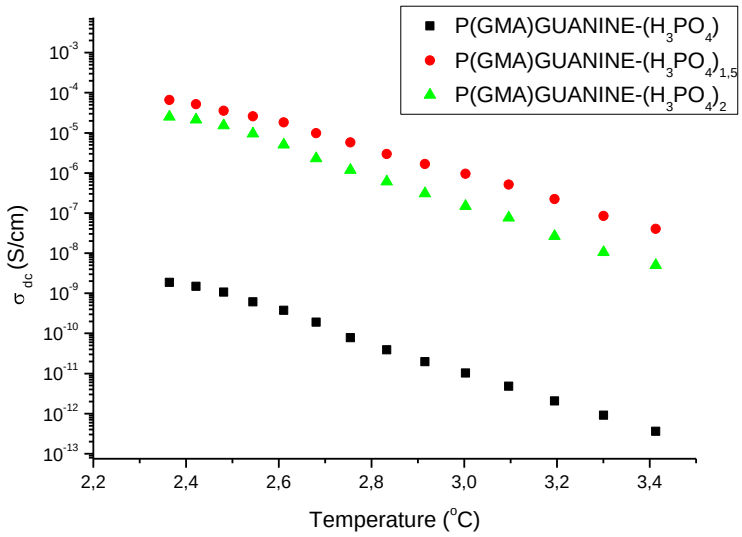

Figure 4.34 DC conductivities of H_3PO_4 doped PGMAGuanine as a function of reciprocal temperature.

There are mainly two transport mechanisms that contribute to the proton conductivity in phosphoric acid doped. The first is the structural diffusion (Grotthuss mechanism) in which the conductivity is mainly controlled by proton transport through phosphate ions, i.e. $H_4PO_4^+$, $H_2PO_4^-$ (Grotthuss proton transport). The second is the vehicle mechanism where the protons travel through the material on a neutral or charged "vehicle". Several studies were reported about the contribution of these mechanisms on the proton conductivity of pure phosphoric acid and it was indicated that the character of conduction mechanism is mainly controlled by the structural diffusion rather than vehicle mechanism (Dippel et al., 1993).

In the phosphoric acid doped PGMAGuanine and PVPA functional PGMAGuanine systems, the doping ratio is highly effective on the proton conductivity of sample which indicates that major part of proton transport is provided over the H_3PO_4 and PVPA as well as over guanine units. Previously, the proton conductivity of acid doped PBI was reported to follow the Arrhenius law, suggesting a hopping-like conduction mechanism (He et al., 2003).

From the conductivity and FTIR results, it can be concluded that the host matrix, PGMAGuanine includes excess phosphoric acid without significant change in the mechanical properties and conductivity occur throughout the material predominantly by Grotthuss mechanism. Among phosphoric acid doped systems, (PGMAGuanine)-$(H_3PO_4)_2$ showed the highest proton conductivity of ~7.04×10^{-5} S/cm at 150 ^oC in the anhydrous state.

4.2 THE IONICAL CROSS-LINKED POLYMER ELECTROLYTES

4.2.1.1 FT-IR Studies of PVTriP(VPA)$_x$

Fig. 4.35 shows the FT-IR spectra of poly(1-vinyl-1,2,4-Triazole), PVTri, polyvinylphosphonic acid, PVPA and the complex polymer electrolytes, PVTriP(VPA)$_x$. In PVTri, the triazole units show several medium or strong peaks in the 1430-1650 cm^{-1} range due to ring stretching (C-N, C=N) vibrations. The peak at 1270 cm^{-1} is due to the ring N-N stretching. The IR spectrum of PVPA shows strong bands at 1040-910 cm^{-1} that belong to asymmetric stretching vibrations of the P-OH group and at 1150 cm^{-1} that corresponds to P=O stretching (Bozkurt and Meyer, 2001). At higher PVPA ratio the P–O–H vibration at 930 cm^{-1} becomes stronger, indicating the existence of excess acidic protons. Additionally, phosphonic acid units give rise to broad bands with medium intensity at 1700-1590 cm^{-1} and 2850-2750 cm^{-1}. The protonation of the 'free' nitrogens of the triazole rings can be observed with the change of the intensity of the peaks within 1200-1520 cm^{-1}. The broad band between 3500 cm^{-1}- 2500 cm^{-1} is the hydrogen bonding network which is necessary for proton conduction (Celik et al., 2008).

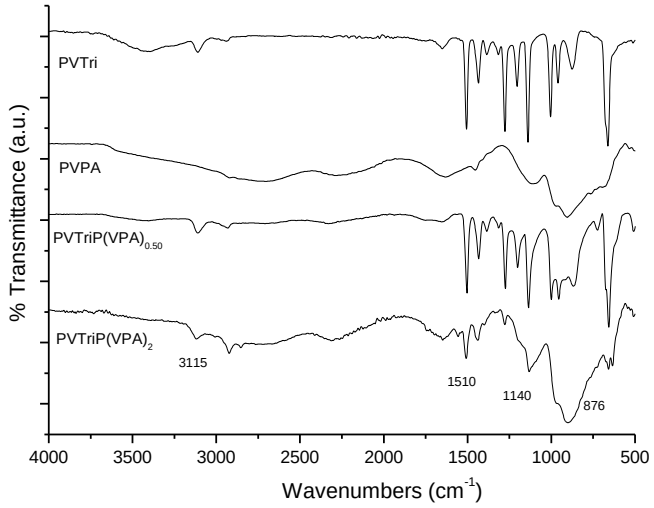

Figure 4.35 FT-IR spectra of the PVTri, PVPA, PVTriP$(VPA)_{0.50}$ and PVTriP$(VPA)_2$.

4.2.1.2 FT-IR Studies of PVTriP$(SSA)_x$

Fig. 4.36 shows the FT-IR spectra of poly(1-vinyl-1,2,4-Triazole) and the polymer electrolytes. In PVTri, the triazole units show several medium or strong peaks in the 1430-1650 cm^{-1} range due to ring stretching (C-N, C=N) vibrations. The peak at 1270 cm^{-1} is due to the ring N-N stretching. The broad absorption band near 1200 cm^{-1} is attributed to asymmetric O=S=O stretching vibration of $–SO_3^-$ groups (Li et al., 2004). The vibration of the phenyl ring substituted with a sulfonic group leads to the peaks at 1005cm^{-1} (Smitha et al., 2006). The deprotonation of the sulfonic acid peak causes the broadening of this peak as well as overlapping with the phenyl ring attached sulfonic anion peak at 1125 cm^{-1} (Li et al., 2004). The protonation of the 'free' nitrogens of the triazole rings can be observed with the change of the intensity of the peaks within 1200-1510 cm^{-1}.

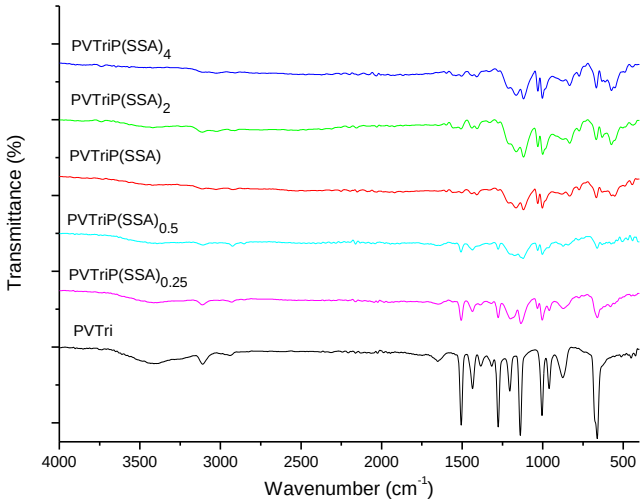

Figure 4.36 FT-IR spectra of the PVTri and PVTriP(SSA)$_x$ (x = 0.25, 0.50, 1, 2, 4).

4.2.2 Solid State ^{13}C CP-MAS NMR Results

4.2.2.1 Solid State ^{13}C CP-MAS NMR Spectra of PVTri

The ^{13}C CPMAS spectra of the pure PVTri is shown in Figure 4.37 In the homopolymer of PVTri, the specific resonances from the different carbon sites can easily be identified. The resonances due to backbone carbons appear at around 40 and 55 ppm. The two ring carbon resonances appear at higher chemical shift values, at 145 and 153 ppm.

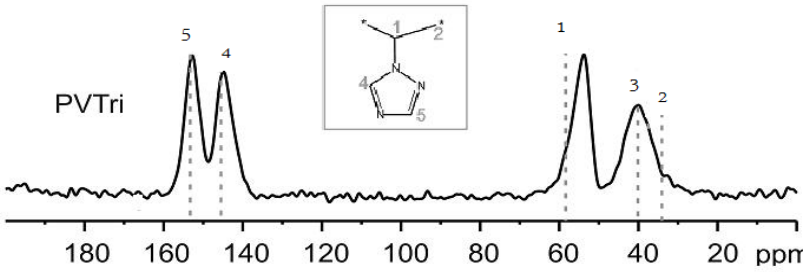

Figure 4.37 The solid state ^{13}C CP-MAS NMR spectrum of PVTri.

4.2.3 SEM Micrographs

4.2.3.1 SEM Micrographs of PVTriP(VPA)$_x$

Surface morphologies PVTriP(VPA) and PVTriP(VPA)$_4$ the complex polymer electrolytes membranes were investigated by scanning electron microscopy (Fig. 4.38 a and Fig. 4.38b). Due to strong interaction between of phosphonic acid groups of PVPA and the triazole units of PVTri, no phase separation occurred during solvent evaporation, hence homogeneous and transparent films formed. This result is also consistent with the DSC curves of blend membranes that no separate T_g transition of impregnated PVTri was observed.

(a) **(b)**

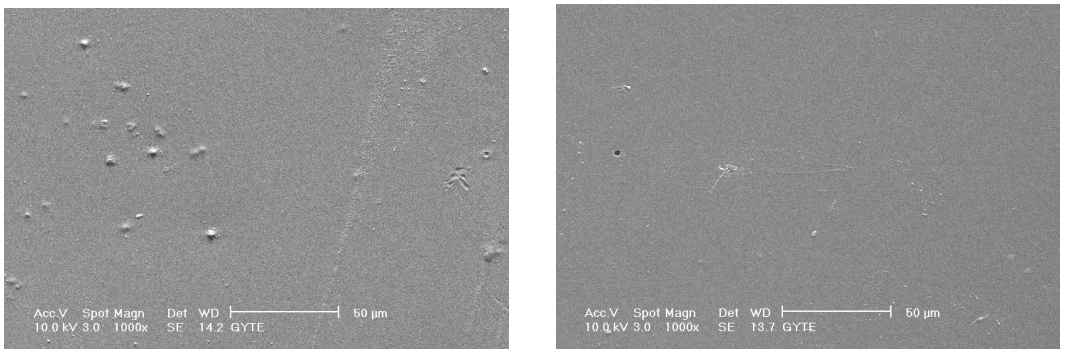

Figure 4.38 SEM micrographs of the surface of (a) PVTriP(VPA), (b)PVTriP(VPA)$_{0.25.}$

4.2.3.2 SEM Micrographs of PVTriP(SSA)$_x$

Surface morphologies PVTriP(SSA)$_2$ polymer electrolytes membranes at different magnifications were investigated by scanning electron microscopy (Fig. 4.39a and Fig. 4.39b). Due to strong interaction between of sulfonic acid groups of PSSA and the triazole units of PVTri, no phase separation occurred during solvent evaporation, hence homogeneous

and transparent films formed. This result is also consistent with the DSC curves of the membranes that no separate T_g transition of impregnated PVTri was observed.

(a) **(b)**

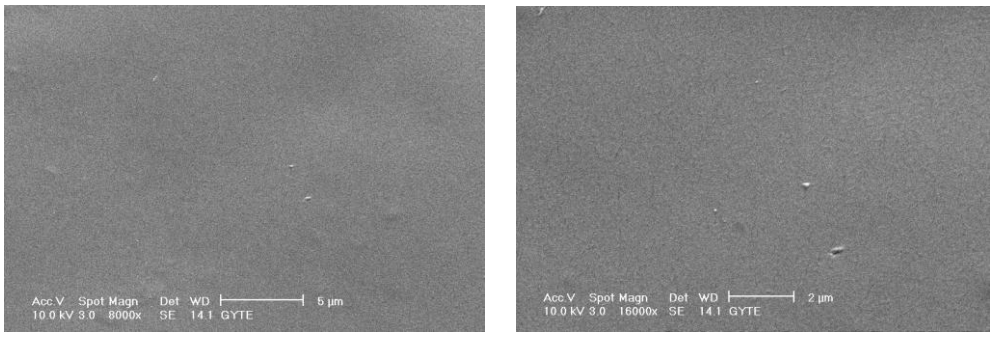

Figure 4.39 SEM micrographs of the surface of PVTriP$(SSA)_2$ (a) 5 μm (b) 2 μm.

4.2.4 TGA analysis

4.2.4.1 TG of PVTriP$(VPA)_x$

Fig. 4.40 shows the thermogravimetry (TG) results of the homopolymer; PVTri has a considerable thermal stability under inert conditions. An exponential weight decay for the PVTri until 200 ^oC can be attributed to loss of absorbed humidity. Above 350 ^oC, a remarkable weight loss derives from the thermal decomposition of triazole groups and the polymer main chain. Both of the complex polymer electrolyte PVTriP(VPA) and PVTriP$(VPA)_2$ illustrate no weight change up to approximately 150 ^oC. Then an elusive weight loss up to 250 ^oC can be attributed to anhydride formation (Celik et al., 2008). Clearly, the dried PVTriP$(VPA)_x$ materials are thermally stable up to 250 ^oC and then they decompose.

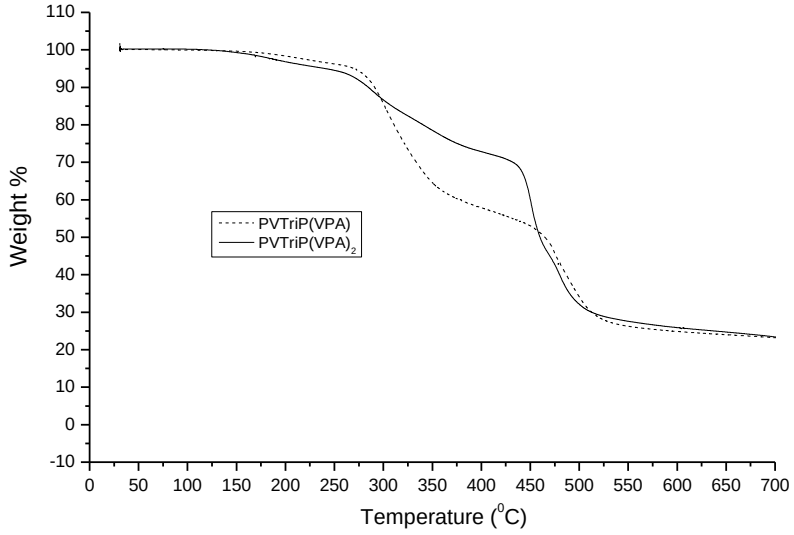

Figure 4.40 TG profiles of the PVTriP(VPA) and PVTriP$(VPA)_2$ under a N_2 atmosphere at a heating rate of 10 ^{0}C/min.

4.2.4.2 TG of PVTriP$(SSA)_x$

Fig. 4.41 and 4.42 show the thermogravimetry (TG) results of the PVTri, PVTriP$(SSA)_1$ and PVTriP$(SSA)_2$ under oxygen and nitrogen atmosphere at a heating rate of 10 ^{o}C/min. Pristine PVTri has a considerable thermal stability under inert conditions. An exponential weight decay for the PVTri until 200 ^{o}C can be attributed to loss of absorbed humidity. Above 350 ^{o}C, a remarkable weight loss derives from the thermal decomposition of triazole groups and the polymer main chain. Both of the complex polymer electrolyte PVTriP(SSA) and PVTriP$(SSA)_2$ illustrate elusive weight loss up to approximately 300 ^{o}C that can be attributed to the absorbed humidity. Clearly, the dried PVTriP$(SSA)_x$ membranes are thermally stable up to approximately 300 ^{o}C then they decompose.

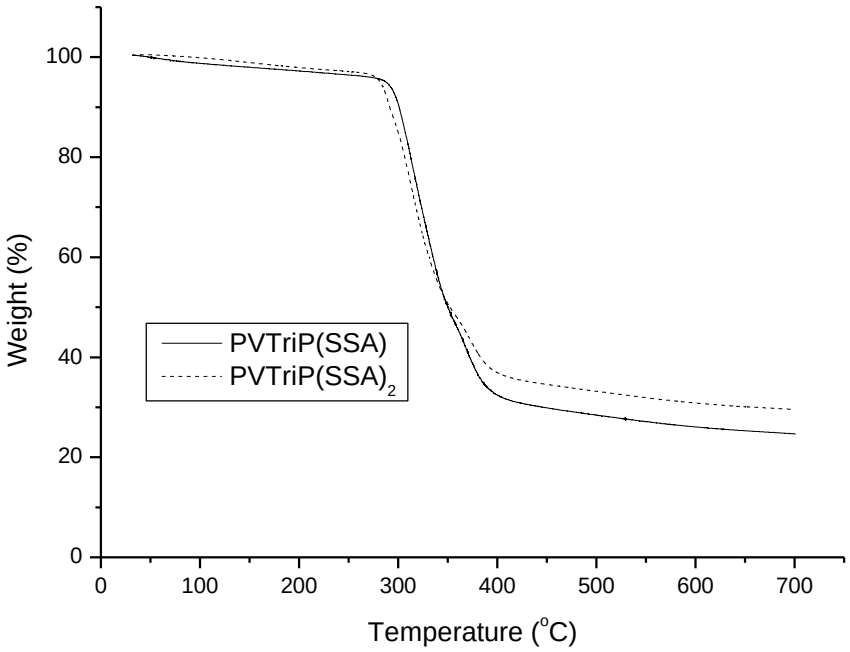

Figure 4.41 TG thermograms of the PVTriP(SSA) and PVTriP(SSA)$_2$ under nitrogen atmosphere at a heating rate of 10 ^{o}C/min.

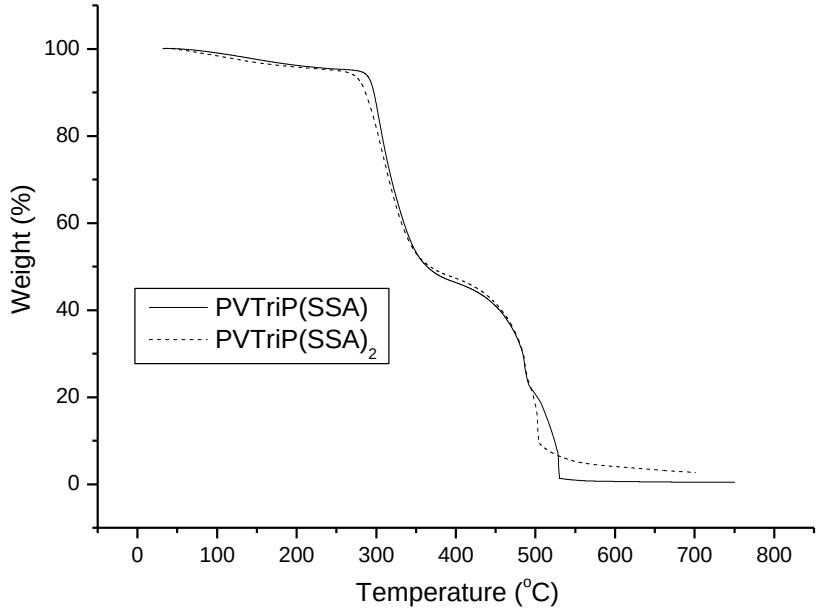

Figure 4.42 TG thermograms of the PVTriP(SSA) and PVTriP(SSA)$_2$ under oxygen atmosphere at a heating rate of 10 ^{o}C/min.

4.2.5 DSC Analysis

4.2.5.1 DSC of PVTriP(VPA)$_x$

Characteristic DSC curves of are PVTriP(VPA), PVTriP(VPA)$_{0.50}$ and PVTriP(VPA)$_2$ shown in Fig. 4.43 The glass transition temperature of the PVTri was reported at around 160 ^oC. PVPA exhibits a glass transition at around -23 ^oC (Celik et al., 2008). The complex polymer electrolytes PVTriP(VPA)$_{0.25}$, PVTriP(VPA)$_{0.50}$ PVTriP(VPA), PVTriP(VPA)$_2$ and PVTriP(VPA)$_4$, have definite glass transition temperatures at 163 ^oC, 145 ^oC,158 ^oC, 140 ^oC, 126 ^oC. The results demonstrated that as the quantity of PVPA increased, the glass transition temperature of the samples shifted to lower temperatures.

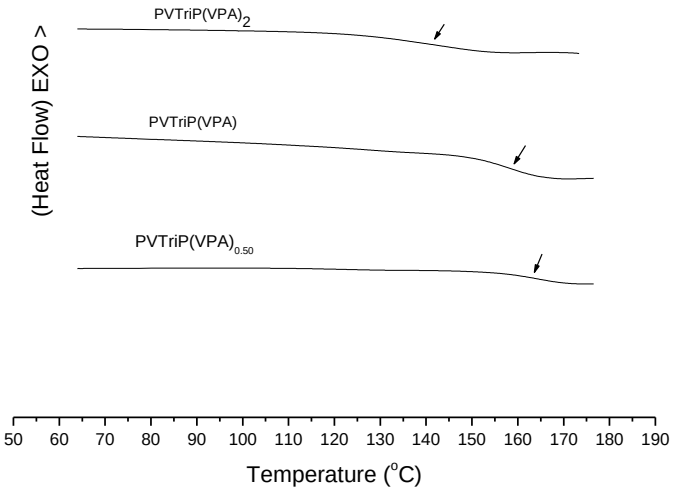

Figure 4.43 DSC traces of PVTriP(VPA), PVTriP(VPA)$_{0.50}$ and PVTriP(VPA)$_2$ recorded under inert atmosphere at a heating rate of 10 ^oC/min.

4.2.5.2 DSC of PVTriP(SSA)$_x$

Differential scanning calorimetry (DSC) was performed to measure the glass transition temperatures of the PVTriP(SSA)$_x$ membranes. Figure 4.44 shows the DSC thermograms of the second heating curves and the corresponding T_g values are depicted in Table 1. All polymer membranes showed one glass transition ranged around 150-160 ^oC, thus homogeneity of the membranes were proved. T_g of pristine PS is nearly 108 ºC. The increase in the glass transition temperatures can be attributed to ionic units as well as the restriction of PSSA polymer segmental motions that may be due to the ionic crosslinking (Li et al., 2004).

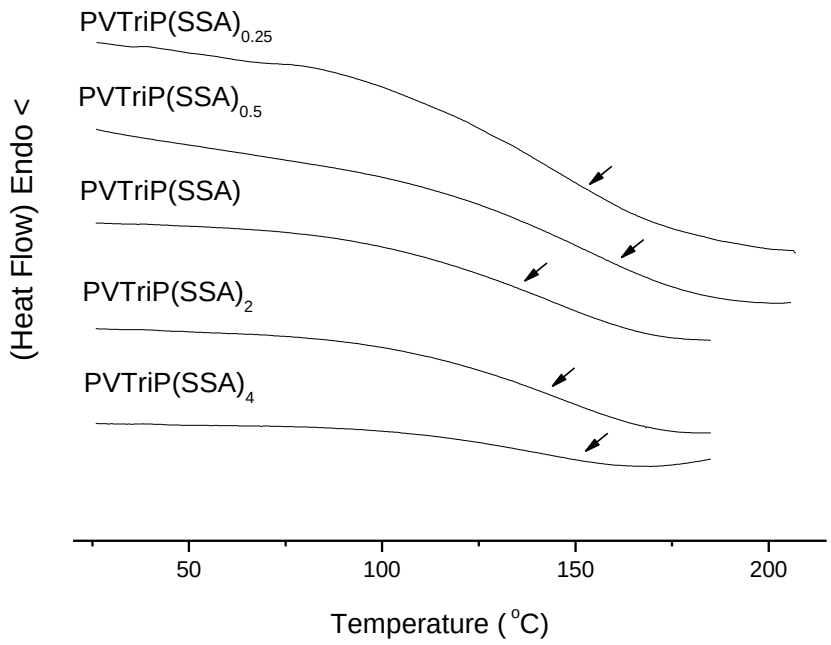

Figure 4.44 DSC curves of the PVTriP(SSA)$_x$ recorded under nitrogen atmosphere at a heating rate of 10 ^oC/min.

4.2.6 Proton Conductivity Studies

4.2.6.1 AC Conductivity Measurements

The AC conductivities, σ_{ac} (ω) of the polymers were measured at several temperatures using impedance spectroscopy. Frequency dependent AC conductivities (σ_{ac} (ω)) were measured using Eq. 1;

$$\sigma'(\omega) = \sigma_{ac}(\omega) = \varepsilon''(\omega)\,\omega\,\varepsilon_o \qquad (1)$$

where $\sigma'(\omega)$ is the real part of conductivity, $\omega = 2\pi f$ is the angular frequency, ε_o is the vacuum permittivity (ε_o = 8.852 x 10^{-14} F/cm), and ε'' is the imaginary part of complex dielectric permittivity (ε^*).

4.2.6.2 DC Conductivity Measurements

The DC conductivity, σ_{dc} is derived from the log scale σ_{ac} versus F curves by linear fitting plateau regions and extrapolating to zero frequency. If the system exhibits Arrhenius behavior, the conductivity isotherm can be fitted by Arrhenius equation (Eq. 2);

$$\ln \sigma = \ln\sigma_o - E_a/kT \qquad (2)$$

where σ_o is the pre-exponential terms, E_a is the activation energy, and k is the Boltzmann constant. If the system follows VTF behavior the curved DC conductivity isotherm can be fitted by Vogel-Tamman–Fulcher-type (VTF) equation (Eq. 3);

$$\log \sigma = \log \sigma_o - E_v/[k(T-T_o)] \qquad (3)$$

where σ_o is the conductivity at infinite temperature, E_v is the Vogel activation energy and T_o is the Vogel temperature.

4.2.6.3 Conductivity of PVTriP(VPA)$_x$

The proton conductivities of anhydrous complex polymer electrolytes were measured from 20 ^{o}C to 180 ^{o}C.

The proton conductivity of all samples was compared in Fig. 4.45-4.52. The conductivity isotherm illustrates that the DC conductivity strongly depends on temperature as well as the ratio of PVPA. The activation energy of PVTriP(VPA)$_2$ was found to be Ea = 0,41 (eV).

The proton conductivity of these samples is improved with PVPA content and maximum proton conductivity was measured for PVTriP(VPA)$_2$ and found to be 2.2x10^{-6} at 180 ^{o}C in the dry state. The proton conductivity of PVTriP(VPA)$_2$ is almost identical with PVTriP(VPA)$_4$, except a slight deviation at higher temperatures. The material with x=2 was considered to be the optimum composition as the complex polymer electrolyte. Conductivity results showed that in the PVTriP(VPA) systems, the PVPA composition is highly effective on the proton conductivity of the samples. Although the major part of proton transport is provided over both phosphonic acid that are coordinated with azoles, the conductivity decrease at higher PVPA containing samples can be attributed to threshold composition of PVPA. Previously, the structure and the local proton mobility of the homopolymer, PVPA were studied by solid-state NMR under fast magic angle spinning (Lee et al., 2007). The study concluded that the proton migration of PVPA is mediated by acidic protons through hydrogen bonding network and condensation of acidic units blocked the proton transport resulting in a decrease in the proton conductivity (Celik et al., 2008).

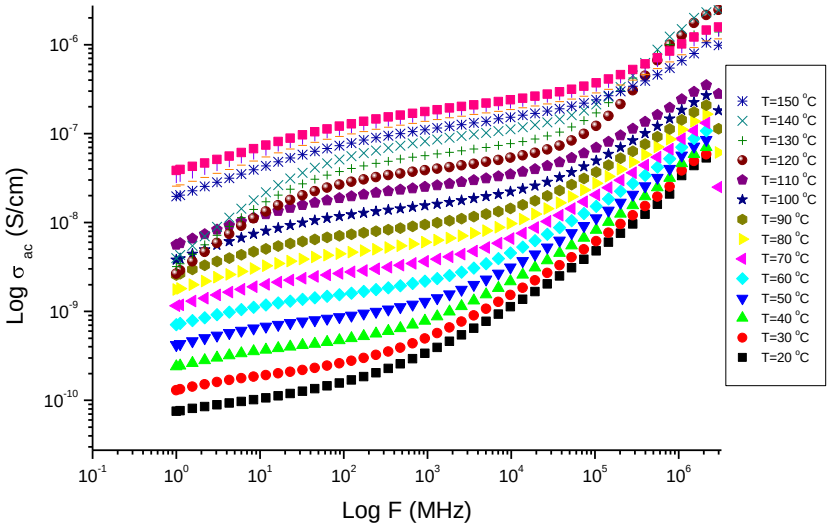

Figure 4.45 AC conductivity versus Frequency (Hz) for PVTriP(VPA) at various temperatures.

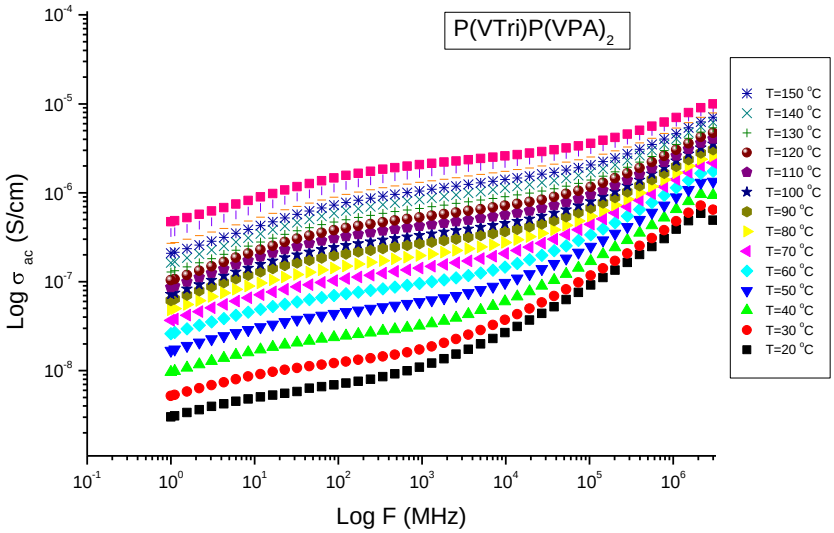

Figure 4.46 AC conductivity versus Frequency (Hz) for PVTriP$(VPA)_2$ at various temperatures.

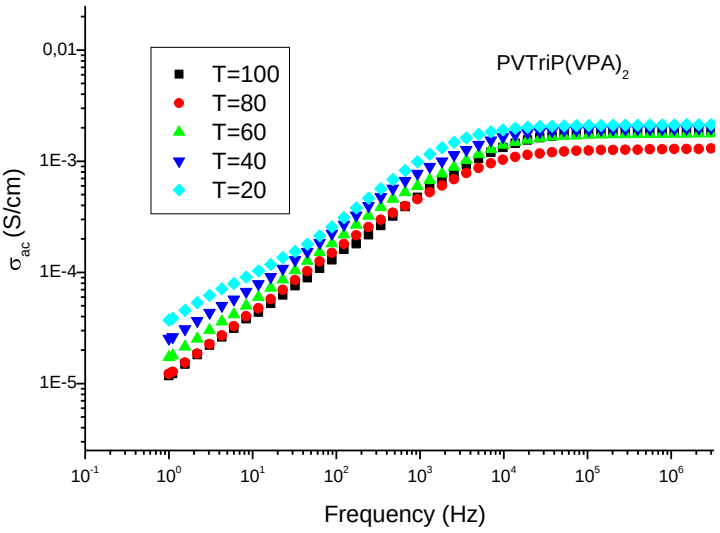

Figure 4.47 Effect of RH (% RH = 50) on ac conductivities of PVTriP(VPA)$_2$ as a function of temperature.

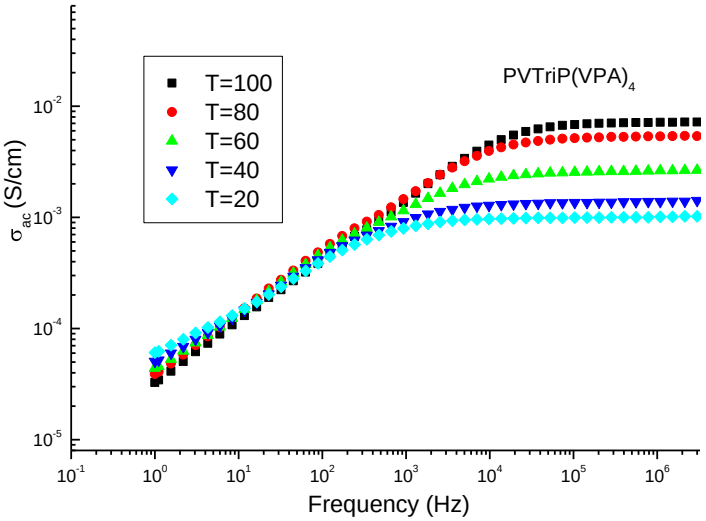

Figure 4.48 Effect of RH (% RH = 50) on ac conductivities of PVTriP(VPA)$_4$ as a function of temperature.

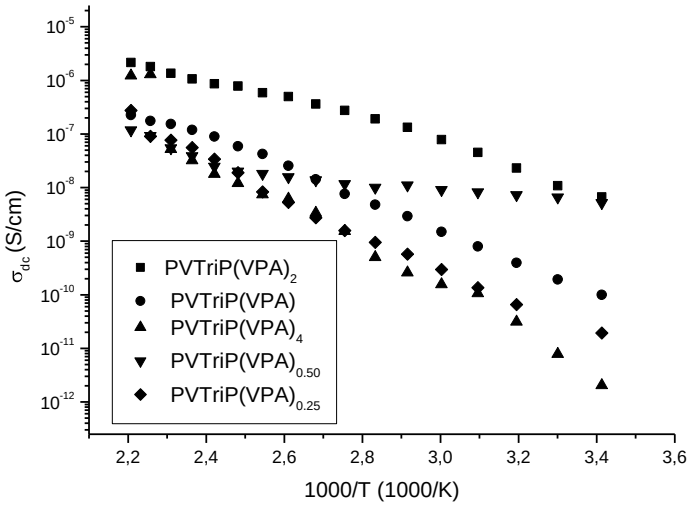

Figure 4.49 The DC conductivity versus reciprocal temperature for the PVTriP(VPA)$_x$ complex polymer electrolytes.

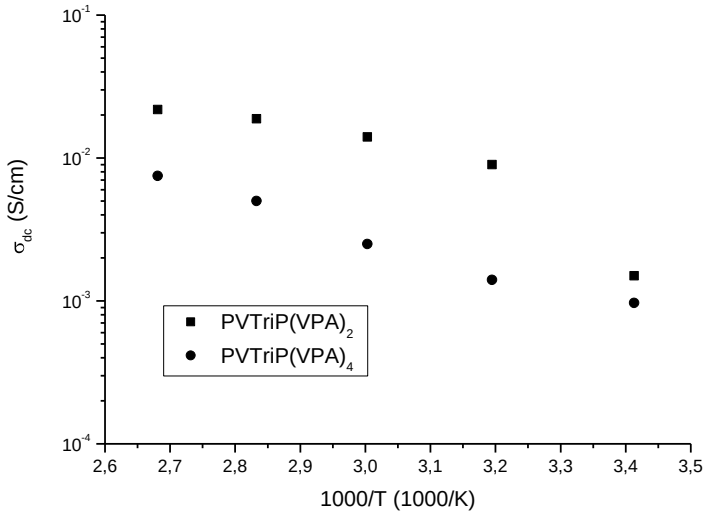

Figure 4.50 Effect of RH (% RH = 50) on proton conductivities of PVTriP(VPA)$_2$ and PVTriP(VPA)$_4$ as a function of temperature.

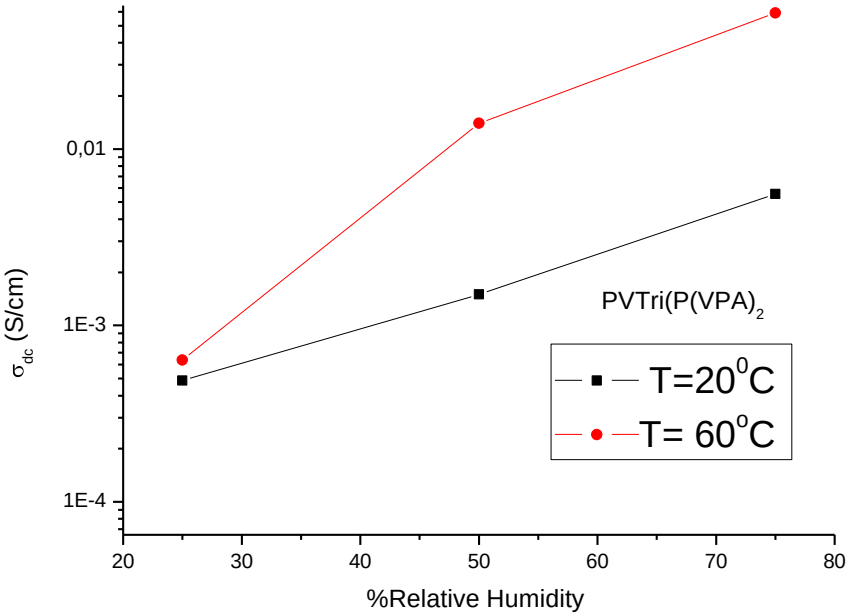

Figure 4.51 Effect of RH content on proton conductivity of PVTrip(VPA)$_{2.}$

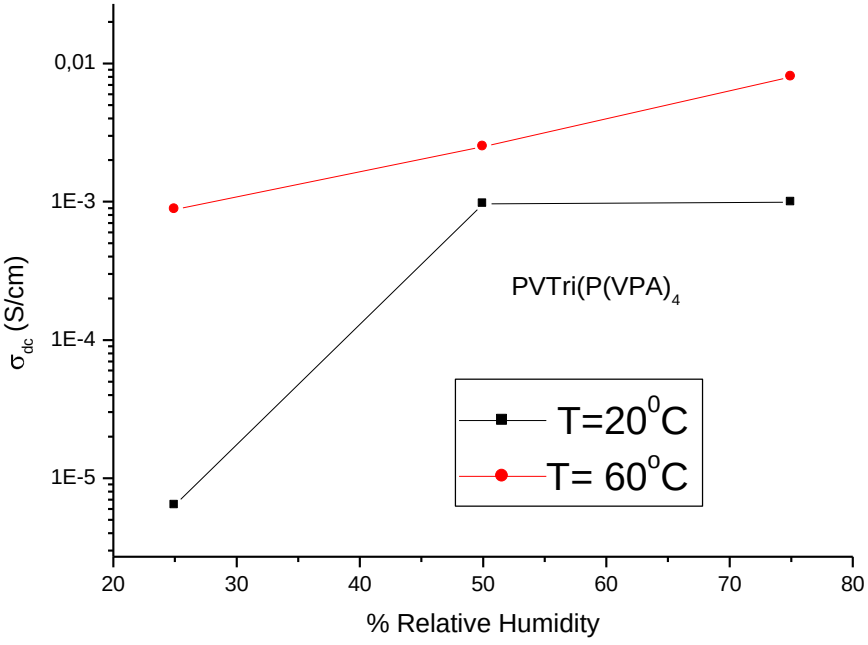

Figure 4.52 Effect of RH content on proton conductivity of PVTrip(VPA)$_{4.}$

The relation between water uptake, self-condensation and proton conductivity of P(VPA) was investigated by Kaltbeitzel *et al* (Kaltbeitzel et al., 2007). They suggested that even after annealing and drying the material, water takes part in the conductivity mechanism. Maximum proton conductivity of pure PVPA 10^{-3} S/cm was reached under 1 bar H_2O atmosphere.

In addition the temperature dependence of proton conductivity of Nafion 117 at several humidity levels was reported in earlier studies (Takimoto et al., 2009, Casciola et al., 2006). The proton conductivity of Nafion 117 membrane was ranged from 0.11 S/cm at room temperature to 0.20 S/cm at elevated temperatures when the membrane is fully humidified. The proton conductivity of Nafion117 at 50 % relative humidity was approximately 0.03 S/cm at 40 ^{o}C (Kaltbeitzel et al., 2007).

The temperature dependence of proton conductivity of humidified PVTriP$(VPA)_2$ and PVTriP$(VPA)_4$ (50% relative humidity) was compared in Fig. 4.50. The proton conductivity of the humidified PVTriP$(VPA)_2$ was measured to be 0.022 S/cm at 100 °C, which is higher than that of PVTriP$(VPA)_4$. It seems that PVTriP$(VPA)_2$ optimum composition and both in humidified and anhydrous form has slightly higher proton conductivity than PVTriP$(VPA)_4$.

Figures 4.51 and 4.52 show the plots of conductivity (in log scale) versus percent relative humidity (RH). Cleary, the conductivity depends on the humidity and increased with increasing water content. For example, the proton conductivity value of both samples with 25 % of RH was approximately 1/100 that of 75 % of RH at 60 ^{o}C. PVTriP$(VPA)_2$ with 75 % RH showed the highest conductivity of about 0.077 S/cm at 80 ^{o}C. Also the humidified sample has better conductivity then pristine PVPA (under 1 bar H_2O atmosphere) which may be due to additional contribution of azoles to the proton conductivity of complex polymer electrolytes via structure diffusion.

4.2.6.4 Conductivity of PVTriP(SSA)$_x$

The conductivities of PVTriP(SSA)$_x$ are shown in Fig. 4.53-4.58. All samples exhibit higher conductivities at high temperature and frequency.

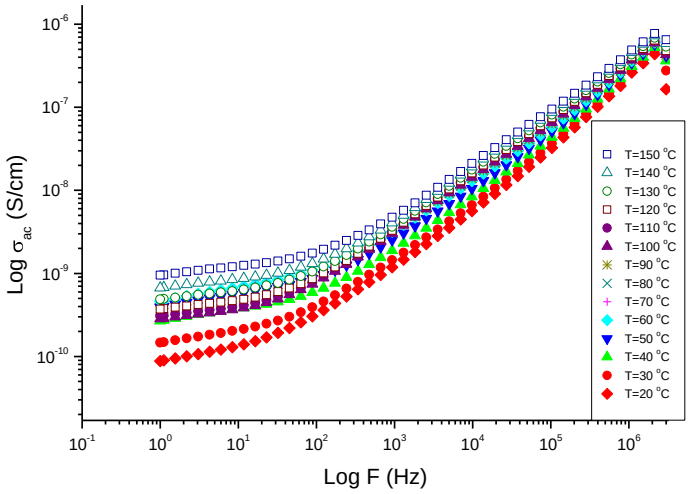

Figure 4.53 AC conductivity versus Frequency (Hz) for PVTriP(SSA) at various temperatures.

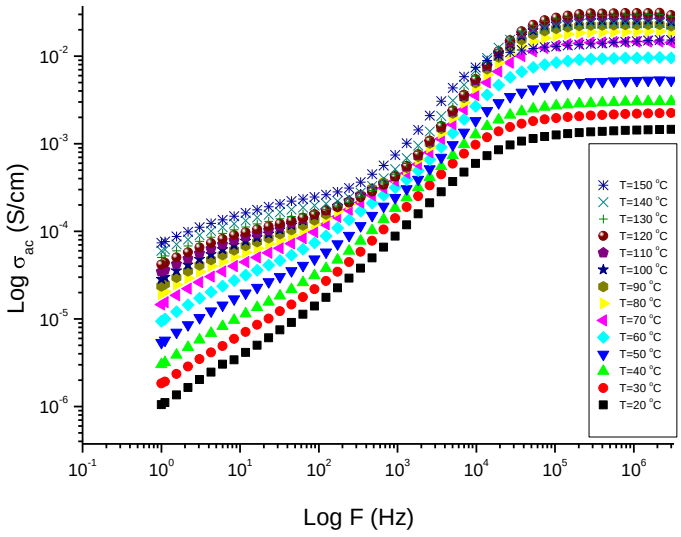

Figure 4.54 AC conductivity versus Frequency (Hz) for PVTriP(SSA)$_2$ at various temperatures.

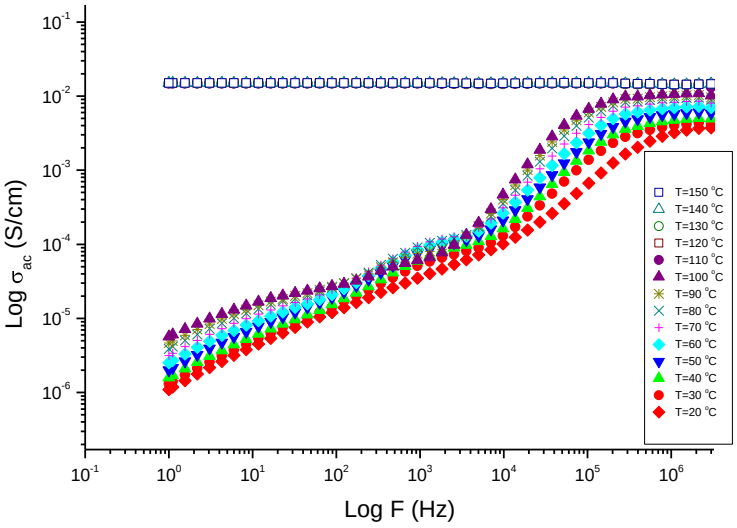

Figure 4.55 AC conductivity versus Frequency (Hz) for PVTriP(SSA)$_4$ at various temperatures.

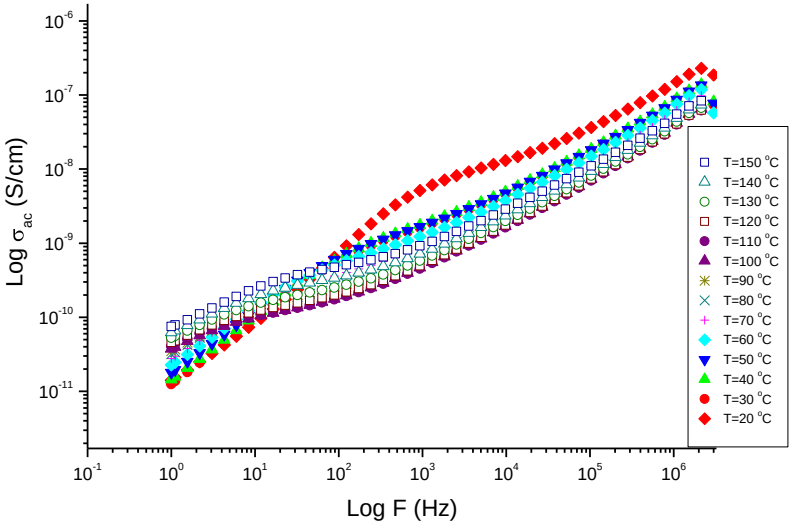

Figure 4.56 AC conductivity versus Frequency (Hz) for PVTriP(SSA)$_{0,50}$ at various temperatures.

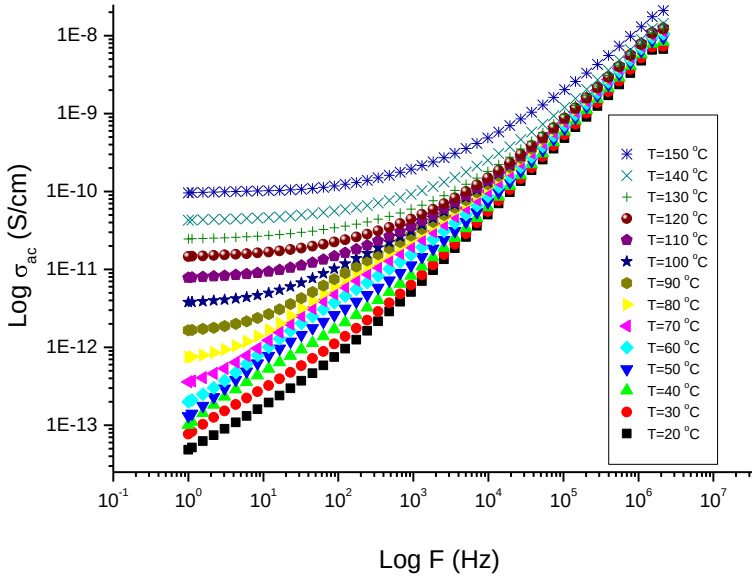

Figure 4.57 AC conductivity versus Frequency (Hz) for PVTriP(SSA)$_{0,25}$ at various temperatures.

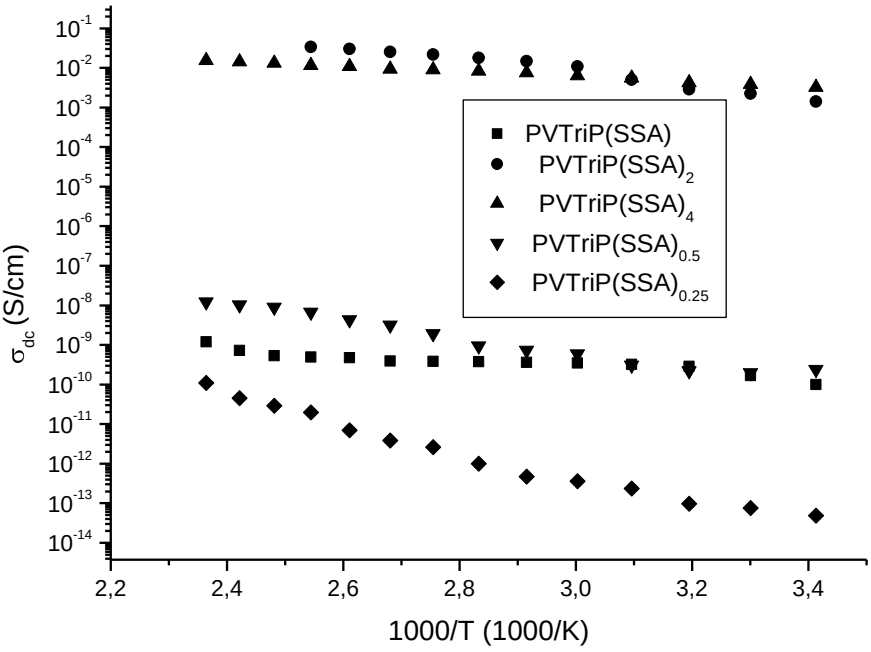

Figure 4.58 DC conductivities of PVTriP(SSA)$_x$ as a function of reciprocal temperature.

The samples were dried under vacuum at 80 ^{o}C for 24 h. Alternating current (AC) conductivity, σ_{ac} versus frequency curves are shown in Fig. 4.54 for anhydrous PVTri:PSSA blend with (1:2) molar ratios. The curves for all the samples involve the frequency dependent and independent areas which are typical in ion conducting polymers. At lower frequencies, an increase in conductivity up to a certain level is due to electrode polarization. Then a frequency independent region over 2-3 decades was observed at higher frequencies. The direct current (DC) conductivity, σ_{dc} of the samples was derived from those plateau regions by linear fitting.

The temperature dependence of proton conductivities for anhydrous PVTri:PSSA blends is shown in Fig. 4.58. As a matter of fact, the conductivity of the PVTri:PSSA system depends on the composition and temperature. The proton conductivity of the samples mainly increases with increasing temperature. The sample with (1:4) and (1:2) molar ratio has high conductivities exceeding 10^{-2} S/cm at high temperatures under completely anhydrous state. At lower molar ratios PSSA is may be used for crosslinking and less free proton contributes to conduction.

Actually, the conduction of the proton can occur through the transition of proton from protonated guest molecules to a non-protonated neighbor host molecule (Munch et al., 2001, Dippel et al., 1993). As reported in the literature, anhydrous polymer systems facilitate the formation of protonic defects and provide strongly labile proton donor and acceptor functions. In addition, acidic molecules such as sulfonic acid could also act as proton donors and acceptors (Dippel et al., 1993). Protonated and non-protonated nitrogen in heterocyclic group of PVTri and sulfonate group of PSSA may act as donors and acceptors in proton transfer reactions. Therefore, both triazole groups of PVTri and sulfonate groups of PSSA act as proton charge carriers. Considering the FT-IR spectra of polymer blend composition as well

as conductivity data, Grotthuss mechanisms (structural diffusion) cause a pathway for the total proton diffusion. The material with x=2 was considered to be the optimum composition as the complex polymer electrolyte. Conductivity results showed that in the PVTriP$(SSA)_x$ systems, the PSSA composition is highly effective on the proton conductivity of the samples. Although the major part of proton transport is provided over triazole units, the conductivity decrease at higher PSSA containing samples can be attributed to protonation of the free nitrogens in the ring. The higher proton conductivity of PVTriP$(SSA)_2$ can be described by the partial protonation of the free nitrogens that is necessary for long range proton transport. However, for the sample PVTriP$(SSA)_4$ there is excess acidic unit and most of the azole rings are protonated, yielding lower conductivity compared to PVTriP$(SSA)_2$. Maximum proton conductivities of 0.015 S/cm at 150 ^oC for PVTriP$(SSA)_4$ and 0.033 S/cm at 120 ^oC for PVTriP$(SSA)_2$ were measured under anhydrous conditions.

4.2.7 Water/Methanol Uptake studies

4.2.7.1 Water/Methanol Uptake of PVTriP$(VPA)_x$

Fig. 4.59 shows the methanol/water solution uptakes of PVTriP$(VPA)_x$. All the materials absorb solvent within 10 min then a threshold is reached which might be due to saturation. Then further swelling of the samples occurs above 30 minute. The swelling character of the polymer complex electrolytes reasonably decreased when there is equimolar of VPA and VTri. This finding is primarily ascribed to ionic crosslinking where the material becomes more rigid when x=1. The reason can be attributed to one to one complexation of triazole with phosphonic acid. At higher compositions of PVTri or PVPA the swelling character of the materials increased.

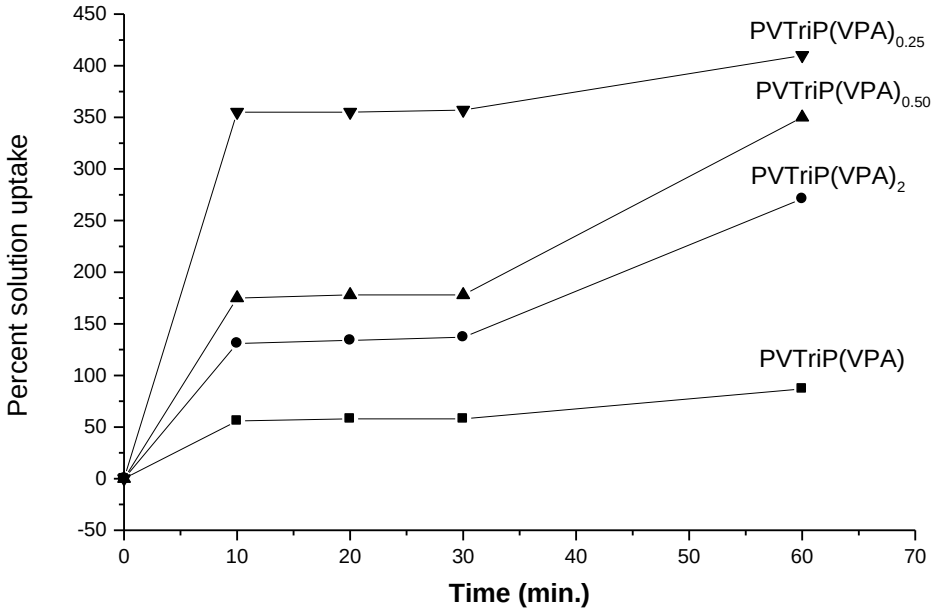

Figure 4.59 Solvent uptakes of PVTriP(VPA)$_x$ (x=1, 2, 0.25, 0.50) at the time of 10-60 min in 12 mol/L methanol/water solution at 25 ^{o}C.

4.2.7.2 Water/Methanol Uptake of PVTriP(SSA)$_x$

Figure 4.60 shows the methanol/water solution uptakes of PVTriP(SSA)$_x$. All the materials except PVTriP(SSA)$_{0.25}$ absorb solvent within 20 min then a threshold is reached which might be due to saturation. Compared the other blend membranes in PVTriP(SSA)$_{0.25}$ ionic crosslinking is less effective and this may lead to continuous swelling. Highest methanol/water uptake was observed for PVTriP(SSA)$_2$ which may be due to the presence of excess PSSA in the matrix. These results demonstrated that the complexation between PSSA and PVTri influenced the solvent uptake character of the final membranes.

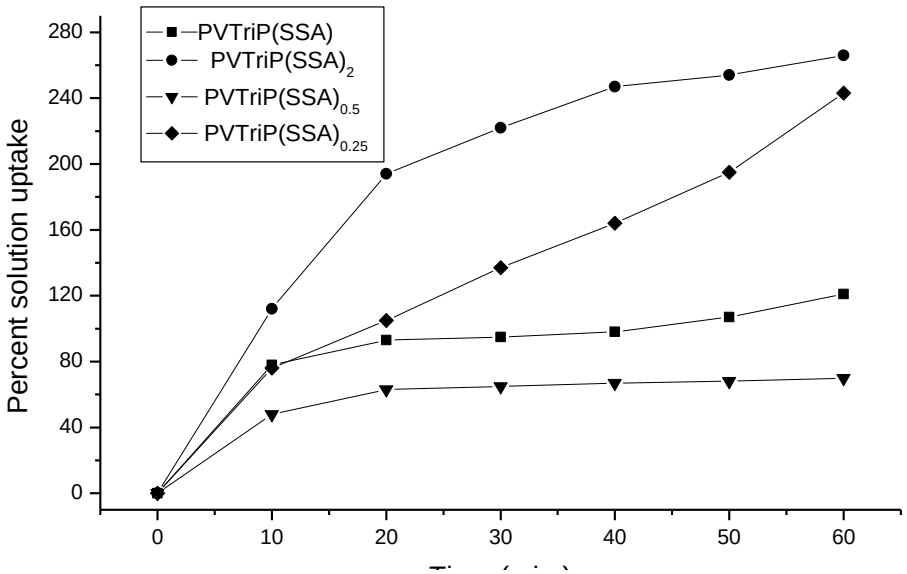

Figure 4.60 Solvent uptakes of PVTriP(SSA)$_x$ (x=1, 2, 0.25, 0.50) at the time of 10-60 min in 12 mol/L methanol/water solution at 25 ^{o}C.

CHAPTER 5

CONCLUSIONS

In the present work, adenine and guanine functional poly(glycidyl methacrylate) polymers have been synthesized. Poly(glycidyl methacrylate) was produced by free radical polymerization of GMA and than adenine and guanine biomolecules were immobilized by ring opening of the epoxide ring. Elemental analysis verified adenine immobilization about 80 % and guanine immobilization about 40 %. The structures of the adenine and guanine functional polymers were proved by FT-IR, solid state ^{13}C CP-MAS NMR, ^{1}H MAS SQ and DQ NMR. Anhydrous proton conducting properties and thermal properties of PVPA functional and phosphoric acid doped PGMAAdenine and PGMAGuanine were investigated. The proton conductivity of the materials increased with dopant concentration and the temperature. However, low conductivity was obtained for PVPA blends polymers. This was attributed to aggregation of the phosphonic acid units in the host matrix which inhibited defect type conduction. DSC and SEM results illustrated the homogeneity of the materials. Phosphoric acid doped polymers showed lower Tg values and higher proton conductivities than PVPA blends system. (PGMAAdenine)-$(H_3PO_4)_2$ and (PGMAGuanine)-$(H_3PO_4)_{1,5}$ showed a maximum water-free proton conductivity of approximately 0.004 S/cm at 150 ^{0}C and 0,007 S/cm at 150 ^{0}C. (PGMAAdenine)-$(H_3PO_4)_2$ and (PGMAGuanine)-$(H_3PO_4)_{1,5}$ membranes can be suggested for application in high temperature polymer electrolyte membrane fuel cells (PEMFC).

As another approach for this study, Poly(1-vinyl-1,2,4-triazole) and poly(vinyl phosphonic acid) was produced by free radical polymerization of the corresponding

monomers. The transparent thin films were produced by complexation of PVPA with the proton exchange reactions between PVTri and PVPA forming ionic crosslinks. TG analysis showed that the samples are thermally stable up to at least 250 °C. DSC and SEM results illustrated the homogeneity of the materials. In the anhydrous state, the proton conductivity of PVTriP$(VPA)_2$ was $2.2x10^{-6}$ at 180 ^oC. The proton conductivity of PVTriP$(VPA)_x$ was increased at 50 % relative humidity and reached to 0.022 S/cm for x=2 and 0.008 S/cm for x=4 at 100 ^oC. The proton conductivity of PVTriP$(VPA)_2$ is approached to that of humidified Nafion 117 membrane at 40 ^oC and at the same humidification level. In this system, the proton diffusion is expected to occur by the transport of the protons through phosphonic acid units up to certain threshold composition of PVPA. PVTri has a comparable thermal stability compared to PBI and complexes of PVPA/PVTri can form free-standing films. After humidification they can be suggested for application in polymer electrolyte membrane fuel cells (PEMFC).

Poly(1-vinyl-1,2,4-triazole), PVTri and poly(styrene sulfonic acid), PSSA was produced by direct sulfonation. Transparent thin films were produced by complexation of PSSA with PVTri at various concentrations to get PVTriP$(SSA)_x$ membranes. FT-IR spectroscopy confirmed the proton exchange reactions between PVTri and PSSA forming ionic crosslinks. TG analysis showed that the samples are thermally stable up to at least 250 °C. DSC and SEM results illustrated the homogeneity of the materials. CV measurement results showed that the stability domain of PVTriP(SSA) extends over 3V. In the anhydrous state, PVTriP$(SSA)_2$ and PVTriP$(SSA)_4$ have higher conductivities of 0.033 S/cm and 0.015 S/cm, respectively. Clearly, conductivity of PVTriP$(SSA)_2$ is approached to that of humidified perfluorosulfonic acid membranes. In this system, the proton diffusion is expected to occur by the transport of the protons through sulfonic acid units up to certain composition of PSSA. PVTri has a comparable thermal stability compared to PBI and complexes of PSSA/PVTri can form free-standing and thermally stable films. PVTri/PSSA based membranes can be suggested for application in high temperature polymer electrolyte membrane fuel cells (PEMFC).

REFERENCES

Agmon N., *Chem. Phys. Lett.*, Vol. 244, pp. 456, 1995.

Agmon N., *J. Chim. Phys*. Vol. 93, pp. 1714, 1996.

Antonucci P.L., A.S. Arico, P. Creti, E. Ramunni, V. Antonucci, *Solid State Ionics*, Vol. 125, pp. 431-437, 1999.

Bozkurt A., M. Ise, K.D. Kreuer, W.H: Meyer, G. Wegner, *Solid State Ionics*, Vol. 125, pp. 225-233, 1999.

Brookman, P. J.; Nicholson, J. W. in: Developments in Ionic Polymers, vol. 2; eds. A.D. Wilson and H. J. Prosser, (Elsevier Applied Science Publishers: London, 1986) pp. 269-283.

Chin D.T., H.H. Chang, *J. Appl. Electrochem.*, Vol. 19, No. 1, pp. 95, 1989.

Costamagna P., S. Srinivasan, *J. Power Sources*, Vol. 102, pp. 242-253, 2001.

Cuddeback R.B., R.C. Koeller, H.G. Drick, *J. Chem. Phys*., Vol. 21, pp. 589, 1953.

Dippel T., K.D. Kreuer, J.C. Lass`egues, D. Rodriguez, Solid State Ionics, Vol.61, No.1–3, pp. 41–46, (1993).

Dippel T., K.D. Kreuer, Solid State Ion., Vol. 46, No. 1-2, pp. 3, (1991).

Dippel Th., K.D. Kreuer, J.C. Lassegues, D. Rodriguez, Solid State Ionics., Vol. 61, pp.41 (1993).

Dippel Th., K.D. Kreuer, J.C. Lassegues, D. Rodriguez, Solid State Ionics., Vol. 61, pp.41 (1993).

Eigen M., ed., Ang. Chem. Intern., (1964).

Erdemi H., A. Bozkurt, W.H. Meyer, Synthetic Metals, Vol. 143, pp.133 (2004).

Gottesfeld, J. Electrochem Soc, Vol. 140, pp. 1-7, (1993).

Goward G.R., M.F.H. Schuster, D. Sebastiani, I. Schnell, H.W. Spiess, J. Phys. Chem. B., Vol. 106, pp.9322 (2002).

Greenwood N.N., A. Thompson, J. Chem. Soc., pp. 3485, (1959).

Grotthuss C.J.D. v., Ann. Chim., LVIII, pp. 54, 1806.

Gunday S.T., A. Bozkurt, W.H. Meyer, G. Wegner, Journal of Polymer Science., Part B: Poly. Phys., Vol. 44, pp.3315 (2006).

Hasiotis C., L. Qingfeng, V. Deimede, J.K. Kallitsis, C.G. Kontoyannis, N.J. Bjerrum, J. Electrochem. Soc., Vol. 148, pp.A513 (2001).

Hasiotis C., Li Qingfeng, V. Deimede, J. K. Kallitsis, C. G. Kontoyannisand N. J. Bjerrum, Journal of The Electrochemical Society, Vol. 148, pp.A513 (2001).

Hickman B.S., M. Mascal, J.J. Titman, I.G. Wood, J. Am. Chem. Soc., Vol. 121, pp.11486 (1999).

Ianniello R., V.M. Schmidt, U. Stmming, J. Stumper, A. Wallan, Electrochim. Acta, Vol. 39, pp. 1863-1869, (1994).

Ismail A.F., N. Zubir, M.M. Nasef, K.M. Dahlan, A.R. Hassan, J. Membrane Sci., Vol. 254, pp.189 (2005).

Kaltbeitzel A., S. Schauff, H. Steininger, B. Bingöl, G. Brunklaus, W.H. Meyer, H.W. Spiess, Solid State Ionics Vol. 178, pp.469 (2007).

Kerres J.A., J. Membrane Sci., Vol. 185, pp. 3 (2001).

Kim J.D., T. Mori, S. Hayashi, I. Honma, Journal of Electrochemical Society, Vol. 154, pp.A290 (2007).

Kreuer K.D., A. Fuchs, M. Ise, M.M. Spaeth, Electrochim. Acta, Vol. 43, pp.1281 (1998).

Kreuer K.D., A. Rabenau, W. Weppner, Angew. Chem.-Int. Edit. Engl., Vol. 21, No. 3, pp. 208, (1982).

Kreuer K.D., J. Membrane Sci., Vol. 185, pp.29 (2001).

Kreuer K.D., Solid State Ion., Vol. 94, No.1-4, pp. 55, (1997).

Kreuer K.D., T. Dippel, W.H. Meyer, J. Maier, Mat. Res. Soc. Symp. Proc., Vol. 293, pp. 273-282, (1993).

Kreuer, K.D., Chemistry Materials, Vol. 8, pp.610–641, (1996).

Kreuer, K.D., Proceedings of the sixth Asian Conference on Solid State Ionic: Science and Technology, 29 November-4 December, pp. 263, New Delhi, (1998).

Lee Y.J., B. Bingöl, T. Murakhtina, D. Sebastiani, W.H. Meyer, G. Wegner, H.W. Spiess, Journal of Physical Chemistry B, Vol. 111, pp. 9711(2007).

Li S., L. Krishnan, S. Srinivasan, J. Benziger, A.B. Bocarsly, J. Membrane Science, Vol. 243, pp.327 (2004).

Li S., Z. Zhou, Y. Zhang, M. Liu, Chemistry of Materials, Vol. 17, pp.5884 (2005).

Ma Y., The Fundamental Studies of Polybenzimidazole/Phosphoric acid Polymer Elevtrolyte for Fuel Cells, Ph. D Thesis, Case Western Reverse University, 2004.

Miyake N., J.S. Wainright, R.F. Savinell, J. Electrochem. Soc., Vol. 148, pp. A898-A904, 2001.

Motupally S., A.J. Becker, J.W. Weidner, J. Electrochem. Soc., Vol. 147, No. 9, pp. 3171-3177, 2000.

Munch W., K.D. Kreuer, W. Silvestri, J. Maier, G. Seifert, Solid State Ionics., Vol. 145, pp.437 (2001).

Munson R.A., J. Phys. Chem., Vol. 68, No.11, pp. 3374–3377, 1964.

Pasupathi S., S. Ji, B.J. Bladergroen, V. Linkov, Int. J. Hydrogen Energy., Vol. 33, pp.3132 (2008).

Rikukawa M., K. Sanui, Prog. Polym. Sci., Vol. 25, pp.1463 (2000).

Schechter A., R.F Savinell. Solid State Ionics, Vol. 147, pp.181 (2002).

Schuster M.F.H., W.H. Meyer, Annu. Rev. Mater. Res., Vol. 33, pp. 233 (2003).

.
Schuster M.F.H., W.H. Meyer, M. Schuster, K.D. Kreuer, Chem. Mater., Vol. 16, pp.329 (2004).

Sen U., S.U. Celik, A. Ata, A. Bozkurt, Int. J. Hydrog. Energ , Vol. 33, pp.2808 (2008).

Sevil F., A Bozkurt, Journal of Physics and Chemistry of Solids, Vol. 65, No.10 pp.1659 (2004).

Shen Y., J. Xi, X. Qiu, W. Zhu, Electrochimica Acta, Vol. 52, pp.6956 (2007).

Smitha B., S. Sridhar, A.A. Khan, J. Membrane Sci., Vol. 259, pp.10 (2005).

Smitha B., S. Sridhar, A.A. Khan, Journal of Membrane Science., Vol. 259, pp. 10 (2005).

Smitha B., S. Sridhar, A.A. Khan, Journal of Power Sources, Vol. 159, pp.846 (2006).

Takimoto N., L. Wu, A. Ohira, Y. Takeoka, M. Rikukawa, Polymer, Vol. 50, pp.534 (2009).

Vink H. A new convenient method for the synthesis of poly(styrenesulfonic acid). Macromol Chem Phys., Vol. 182, pp.279 (1981).

Wainright J.S., J.T. Wang, D. Weng, R.F. Savinell, M. Litt, J. Electrochem. Soc., Vol. 142, pp.L121 (1995).

Watkins DS. In: Blomen LJMJ, Mugerwa MN, editors. Fuel cell systems, New York: Plenum Press, pp. 493, 1993.

Wycisk R., J. Chisholm , J. Lee, J. Lin, P. N. Pintauro, Journal of Power Sources, Vol. 163, pp. 9 (2006).

Xing B.Z., O. Savadogo, Journal of New Materials for Electrochemical Systems, Vol. 2, pp.95 (1999).

Yamada M., I. Honma, Electrochim. Acta, Vol. 48, pp.2411 (2003).

Yamada M., I. Honma, Polymer, Vol. 45, pp.8349 (2004).

Yang C., P. Costamagna, S. Srinivasan, J. Benziger, A.B. Bocarsly, J. Power Sources, Vol. 103, pp.1 (2001).

Yeager H.J, A. Eisenberg, in: Perfluorinated Ionomer Membranes; eds. A. Eisenberg and H. L. Yeager, ACS Symp. Ser. No.180, (American Chemical Society: Washington,DC, 1982) pp. 1-6, 41-63.

Zhang H., X. Li, C. Zhaoa, T. Fua, Y. Shi and Hui Na, Journal of Membrane Science, Vol. 308, pp.66 (2008).